PLASMA EXTRACELLULAR VESSICLES, EXERCISE RESISTNACE AND CANCER

A Dissertation

SUBMITTED TO THE FACULTY OF THE UNIVERSITY OF MINNESOTA BY

Patrick Vanderboom

IN PARTIAL FULFILLMENT OF THE REQUIERMENTS FOR THE DEGREE OF DOCTOR
OF PHILOSOPHY

Dr. Surendra Dasari, Advisor

July 2021

Abstract

Extracellular vesicles (EVs) are released into blood from multiple organs and carry molecular cargo that facilitates inter-organ communication and an integrated response to physiological and pathological stimuli. Interrogation of the protein cargo of EVs is currently limited by the absence of optimal and reproducible approaches for purifying plasma EVs that are suitable for downstream proteomic analyses. We describe a size exclusion chromatography (SEC)-based method to purify EVs from platelet poor plasma (PPP) for proteomics profiling via high-resolution mass spectrometry (SEC-MS). The SEC-MS method identified more proteins with higher precision compared to several conventional EV isolation approaches. We applied the SEC-MS method to identify the unique proteomic signatures of EVs released from platelets, adipocytes, muscle cells, and hepatocytes, with the goal of identifying tissue-specific EV markers. Further, we applied the SEC-MS approach to evaluate the effects of endurance and resistance exercise on EV proteomic cargo in human plasma.

A prerequisite to studying the role of EVs in metabolic disorders such as type 2 diabetes is an in-depth understanding of the molecular mechanisms involved in dysregulation of insulin sensitive tissues such as skeletal muscle. In line with this, we utilized a multi-omics approach to characterize mechanisms underpinning exercise resistance in obese individuals. In this study we characterized the difference in the response to acute exercise between healthy subjects and individuals with chronic inflammation using skeletal muscle biopsy samples. This study identified dysregulation of diverse signaling

pathways, including glycogen synthesis, myogenesis and AMPK signaling in obese individuals.

Finally, we utilized the biomarker potential of SEC-MS to identify differences in protein abundance and composition in EVs isolated from individuals with the hematological malignancy multiple myeloma (MM) and its precursor disease multiple myeloma of undetermined significance (MGUS). This analysis found that CD71 was upregulated in small and large EVs in individuals with MM relative to MGUS, suggesting that iron utilization and homeostasis in the tumor micro environment may play a role in disease progression. Additionally, CD40 was upregulated in individuals with standard cytogenetik risk MM relative to MGUS but was not identified in individuals with high risk MM suggesting that adaptive immune function is correlated to cytogenetic risk. These proteins hold the potential to be useful biomarkers to monitor disease progression in the clinic.

Table of Contents

List of Tables Page

List of Figures Page

Chapter 1

INTRODUCTION

Integrated physiology relies on proper communication between different tissues, and interest in extracellular vesicles (EVs) has grown rapidly in recent years, owing to their role in cell-to-cell communication (Colombo et al., 2014; Guay and Regazzi, 2017; van Niel et al., 2018). EVs are a diverse group of membrane vesicles consisting of two major categories, exosomes and microvesicles. Exosomes range in size from of ~40 to 160nm and are of endosomal origin, whereas microvesicles can be much larger (~50nm to1µm) and bud directly from the plasma membrane (1). EVs of all size types contain protein, nucleic acid, and lipid cargo (Korutla et al.; Minciacchi et al., 2015; van Niel et al., 2018) and exosomes, in particular, have been shown to exchange these molecules between cells to facilitate tissue cross talk. In this thesis, the term EVs will be used to refer to vesicles in the size range of exosomes unless otherwise mentioned.

Several areas of research are actively investigating the role of EVs in intercellular communication and coordinated response to physiologic and pathologic stimuli. One such field is exercise physiology, where recent work has associated the release of EVs from skeletal muscle and other tissues during exercise (2). Regular exercise is known to improve health and reduce the risk of many diseases including type 2 diabetes, obesity, hypertension and some forms of cancer (3,4). The mechanisms underpinning the systemic health benefits of exercise, however, are largely unknown (5). Recent literature suggests that EVs function

in an autocrine/paracrine or endocrine manor to mediate the systemic benefits of exercise (6). A critical first step in elucidating the role that EVs play in mediating the health benefits of exercise via intercellular communication is fully characterizing the protein cargo of EVs released during exercise. Although efforts have been made to characterize EVs released after exercise (7), methodological limitations including the use of non-platelet depleted plasma limit the reach of their findings.

As mediators of intercellular communication, EVs are also involved in the pathogenesis of many diseases. EVs associated with obesity, a known risk factor for several diseases including diabetes, heart disease stroke and cancer (8,9), have been shown to modulate glucose and lipid metabolism (10) and are thought to mediate aspects of obesity-related insulin resistance (11), a primary factor in the etiology of type 2 diabetes. Although a considerable amount of resources have been devoted to studying the role of obesity related EVs in the development of metabolic disorders, large knowledge gaps remain. Prior to understanding the role of obesity associated EVs in metabolic disorders such as diabetes and anabolic resistance, mechanisms of local pathway dysregulation in insulin sensitive tissues such as skeletal muscle need to be further characterized.

Several derangements in skeletal muscle are associated with obesity, including mitochondrial impairments, oxidative stress, insulin resistance, weakness, and fatigue. Exercise has been shown to improve these impairments, however, a significant percentage of individuals (15-20%) fail to realize the health benefits even when interventions are carefully controlled (12-15). This phenomenon, referred to as exercise resistance, is particularly prevalent in older and obese adults. These individuals display impaired protein

synthesis rates and anabolic responses following exercise and nutrition (16-18), which are probable contributing factors to the attenuation of adaptive responses to exercise. In this work, we utilized a multi-omics approach to characterize the differential response to exercise between lean and obese individuals with the goal of identifying dysregulated pathways that contribute to exercise resistance. This work will lay the foundation for future studies that aim to characterize the effect of EVs associated with obesity and their involvement in metabolic disorders.

Another promising field of EV research is cancer, where growing evidence suggests that EVs play a critical role in tumorigenesis (19). In multiple myeloma (MM), there is an intense interest in EVs within the bone marrow micro environment (BMM) and their role in MM pathogenesis (20,21). It is now well established that alterations in the BMM facilitate tumor growth, angiogenesis bone disease and immune evasion (20-22) which promote disease progression, however, the role that EVs play in this process remains unclear and requires further characterization.

To understand the role of EVs in physiological and pathological states, reliable and reproducible profiling of circulating EV molecular cargo is critically important. Interrogation of plasma EV protein cargo, however, is currently limited by the absence of optimal and reproducible approaches for purifying EVs from plasma that are suitable for downstream proteomic analyses. This thesis describes the development of a size exclusion chromatography (SEC)-based method to purify EVs from platelet poor plasma (PPP) for label-free proteomic analysis via high resolution mass spectrometry (SEC-MS). The quantitative performance of SEC-MS was established and compared to the current gold

standard, differential ultracentrifugation (UTC). We then applied SEC MS to characterize the abundance and composition of EVs released after single bouts of endurance and resistance exercise. Further, we performed a multi-omics study to characterize differences in the response to exercise between lean and obese individuals in skeletal muscle. This study will pave the way for future studies that aim to characterize the role of EVs in metabolic disorders. Finally, we utilized SEC-MS to identify EV based biomarkers of disease biology in patients with the hematological malignancy multiple myeloma (MM). The identified biomarkers have the potential to predict which patients are at risk of progressing from the precursor disease, multiple myeloma of undetermined significance (MGUS), to MM. If validated, these biomarkers will fill a critically needed role in the clinic (23) which will directly benefit these patients.

CHAPTER 2

Development and characterization of a platform for proteomic analysis of EVs isolated from plasma. EVs are membranous structures released from most cells that serve as vehicles to exchange protein, nucleic acid, and lipid cargo (24-26) between distant organs to facilitate intercellular communication. In order to characterize the protein cargo of EVs isolated form plasma, improved isolation techniques are required. Currently, a variety of approaches are used by investigators to purify EVs from plasma (27), including ultracentrifugation and commercial kit-based isolations. Many of these methods suffer from poor reproducibility or incompatibility with downstream analytical approaches, highlighting the need to establish a robust and reproducible approach for purifying plasma EVs to allow in-depth characterization and accurate quantification of their molecular content.

While EVs derived from cell culture media can be isolated with high purity and in relatively large amounts (28), isolation of plasma derived EVs pose several unique technical and analytical challenges. For example, proteomic characterization of plasma derived EVs isolated with differential ultracentrifugation (UTC) has been confounded by the co-isolation of an overwhelming number of plasma protein contaminants (29,30). Proteomic analysis of EVs is also limited by notoriously low isolation yield due to EV loss associated with successive washing steps (31). Alternative approaches include commercially available kits based on membrane affinity (32), polymer precipitation (33), and immunoprecipitation (34). While these methods are suitable for some types of

downstream analyses, they are also incompatible with unbiased, in-depth characterization of EV proteins. Size exclusion chromatography (SEC) based EV isolation was reported to rapidly isolate relatively pure EVs from plasma (35-37), and shown to produce exosomes that are suitable for downstream proteomics analysis (38,39). Although this method is promising, post isolation processing methods need to be developed to allow for in-depth characterization of plasma EV cargo. Furthermore, optimized pre-analytical methods need to be coupled with sensitive high-resolution mass spectrometry analysis to achieve precise relative quantification of proteome differences between groups. Finally, there is a need to benchmark the analytical performance of the SEC method relative to other EV isolation approaches to serve as a resource for those interested in EV proteomics research.

Another technical challenge of investigating plasma-derived EVs is the contribution of platelets, which are believed to contribute 70-90% of circulating EVs and are known to release EVs *ex vivo* when activated during sample handling procedures. A particularly problematic issue is the several-fold increase in plasma EV concentration caused by platelets upon cooling/freezing (40,41). This is especially important because cooling/freezing is a necessary pre-analytical step when analyzing a large number of plasma samples that require some interim storage. To address this issue, rigorous pre-analytical guidelines have been established by the International Society of Extracellular Vesicles (ISEV) and International Society on Thrombosis and Haemostasis (ISTH) to limit *ex vivo* generation of platelet EVs (40,42-44).

In the current study, we systematically evaluated an innovative approach using SEC coupled to high-resolution mass spectrometry (SEC-MS) for comprehensive proteomic characterization of human plasma EVs. We address several important factors, including sample purity, method reproducibility, and downstream mass spectrometry analysis that are important for characterizing the EV protein cargo of large sample groups in both research and clinical settings. We also demonstrate the importance of following the rigorous pre-analytical guidelines established by the ISEV and ISTH to limit *ex vivo* generation of platelet EVs (40,42-44). Additionally, sample processing steps downstream of EV isolation require careful attention due to the challenging nature of these samples. Finally, we address the lack of a benchmark for plasma EV proteomics method reproducibility and quantitative performance. Toward this goal, we provide an optimized and reproducible method for isolating plasma EVs from human plasma that is suitable for downstream analysis of protein cargo. To demonstrate the sensitivity of this analytical approach to detect physiological changes in exosome proteomic cargo, we evaluated the effects of acute exercise on proteome cargo of EVs isolated from human plasma samples.

Results

SEC Improves Plasma EV Proteomics Characterization. SEC is a low-resolution, size-based, fractionation technique. Larger EVs do not interact with the SEC resin and pass through the column rapidly, whereas smaller particles (e.g., plasma proteins) interact with the resin and pass through at a slower rate. This separation enables improved proteomic characterization of EVs (38,39), largely by increasing isolation yield and

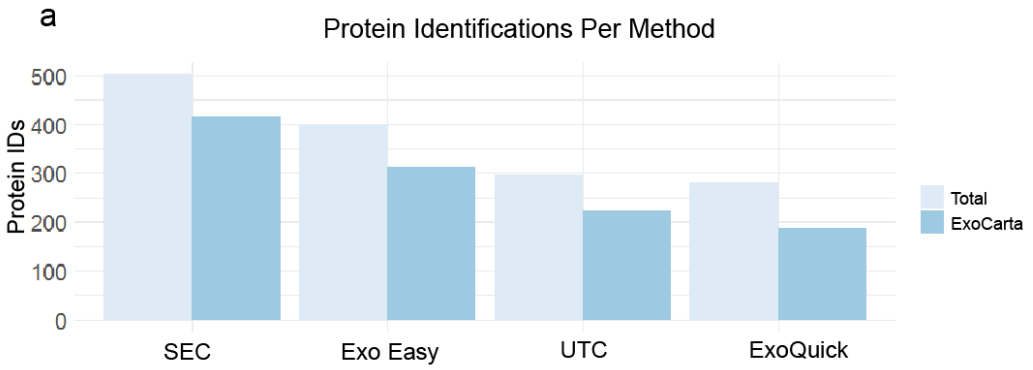

b

	CD9	CD81	CD63	PDCD6IP	ADAM10	SDCB1	FLOT1	ANXA5	OIT3
ExoEasy	x	x	-	-	-	x	-	-	-
ExoQuick	-	-	-	-	-	-	-	-	-
SEC	x	x	-	x	x	x	x	x	x
UTC	x	x	-	-	-	x	-	-	-

Figure 1. Size exclusion chromatography (SEC) improves plasma EV Proteomics Characterization. (A) Four commonly used methods were used to isolate EV's from plasma of an individual healthy participant in the rested state for proteomics characterization. The highest number of total proteins (light blut bar) and proteins associated with the exocarta database (dark blue bar) were identified using SEC. (B) SEC also identified more EV marker proteins compared to the other methods.

reducing plasma protein contamination (45). We investigated the proteomic profiling compatibility of plasma EVs that were isolated with SEC compared to several conventional plasma EV isolation methods. We used platelet poor plasma (PPP) collected from a healthy donors in the resting state following overnight fast to reduce *ex vivo* contribution of platelets to the plasma EV population. PPP was prepared as previously described (46) with modifications (see methods). EVs were also isolated from PPP by differential ultracentrifugation (UTC), SEC (qEV Original), polymer precipitation (ExoQuick), and membrane affinity (ExoEasy). We show that SEC outperformed other methods, based on the ability to detect greater numbers of exosome proteins (defined by the Exocarta

database; **Figure 1A**). Furthermore, SEC identified more canonical EV marker proteins (28) from less sample volume when compared to the UTC and ExoEasy methods (**Figure 1B**).

SEC-coupled mass spectrometry can reproducibly distinguish EV-associated proteins from plasma contaminants. To further characterize and optimize the SEC-MS assay, we analyzed the elution patterns of canonical EV marker proteins and plasma contaminants using SEC. Fasting PPP (2 mL) was obtained from a donor, and plasma EVs were isolated using a qEV2 SEC column (Izon Science, Christchurch, NZ). We collected individual 1 mL SEC fractions spanning the region where EVs elute from the SEC column (fractions 12-22) and processed them individually with a label-free proteomics workflow (see Methods). The intensities of six canonical EV marker proteins measured in sequential SEC column fractions were used to generate SEC EV elution profiles (**Figure 2A**). The elution profiles of all six EV marker proteins show distinct peaks that co-eluted over seven distinct SEC fractions (fractions 15-21) (**Figure 2A**). High molecular weight plasma protein contaminants such as fibrinogen, apolipoprotein B and IgM, also eluted in this region, however, the peak profiles of these common plasma contaminant proteins were right-shifted (**Figure 2A**), thereby differentiating them from the well-resolved EV marker SEC peaks. These results indicate that SEC can effectively separate exosomes from plasma contaminants.

Orthogonal separation of the EVs and plasma contaminants by SEC was used to refine the method and develop an algorithm to flag potential plasma contaminants in EV

SEC-MS experiments. Toward this goal, a reference elution range was established for EVs using the ExoCarta top 100 (ECT100), a list of the most commonly observed proteins in exosomes (47). 79 of 84 ECT100 proteins detected displayed Gaussian shaped profiles which reached their intensity apex, an indicator of maximum abundance, between fractions 17 and 19 (**Figure 2B, C**). The five ECT100 proteins that reached intensity apexes outside of fractions 17-19 exhibited chromatographically distinct peak profiles (data not shown) that were mainly associated with the delayed elution of plasma contaminants, rather than EV derived proteins. These proteins also have high molecular weights and high plasma concentrations (A2M, FN1) or the ability to form multi-molecular complexes (THBS-1 and LGALS3BP) (48,49). The large size and chromatographic association with plasma contaminants suggests that these proteins may be of plasma origin, rather than EV derived. Consistent with this concept, serum albumin, a known plasma contaminant and ECT100 protein, exhibited an elution profile that was distinct from all other ECT100 proteins. Further review of all proteins co-eluting with albumin revealed that none of them were associated with ECT100, and that fraction contained several abundant erythrocyte proteins such as hemoglobin, band 3 anion transport protein, and peroxiredoxin-2 (50). These observations suggest that erythrocyte fragments and large protein aggregates containing albumin elute before EVs. Hence, we determined that the reference EV SEC elution range was between fractions 17 and 19 and all proteins in the dataset with an apex falling within this fraction range were extracted and categorized as "EV-associated proteins." Finally, high molecular weight proteins (> 200kDa), proteins known to form large complexes (immunoglobulin, apolipoproteins, complement), and common contaminants (keratin &

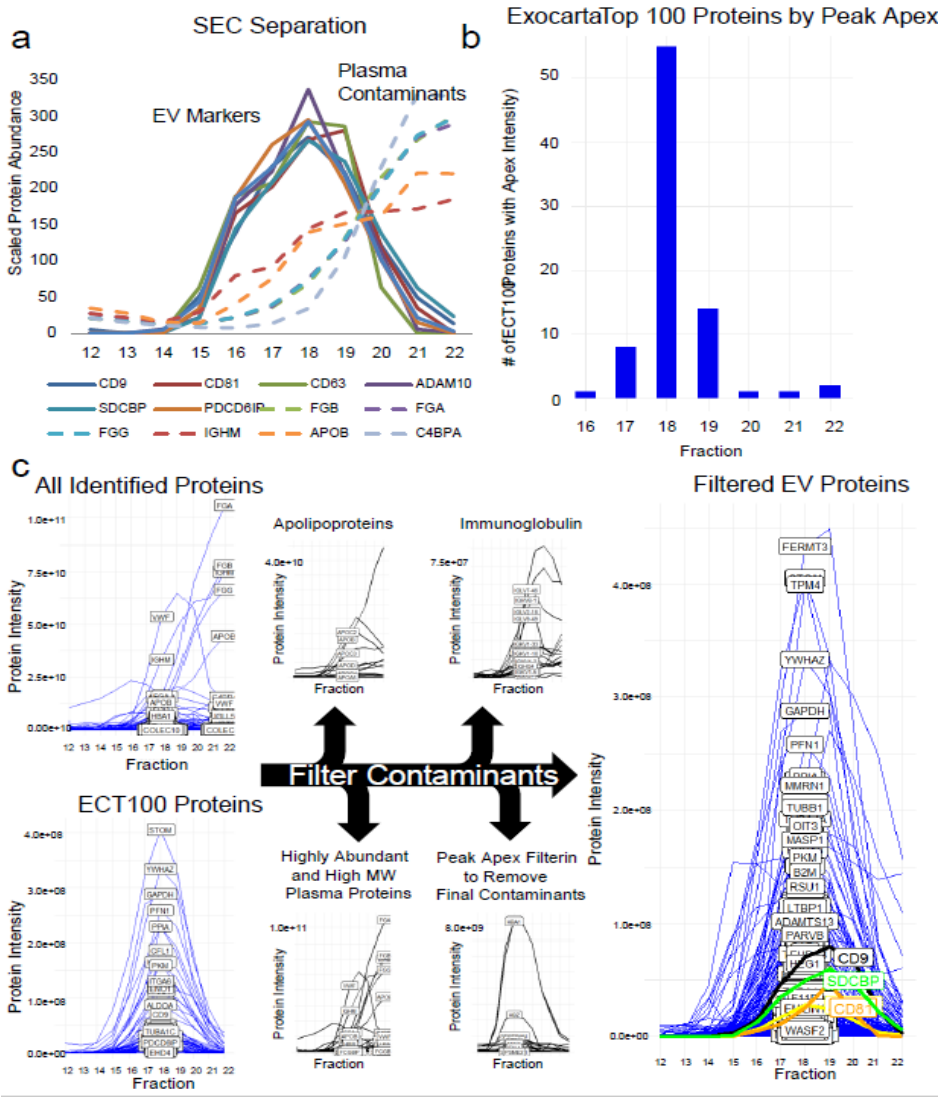

Figure 2. SEC separation of EV's from plasma proteins. (A) SEC fraction profiles of several EV markers and high molecular weight plasma proteins to illustrate separation of EV's from plasma proteins. Profiles are generated from protein intensities of individually analyzed 1ml fractions across the EV elution range. (B) Bar plot of intensity apex vs SEC fraction for proteins in the Exocarta top 100 (ECT100) show where EV's are eluting from the SEC column. (C) Schematic of a bioinformatics based filtering process to identify potential contaminant proteins. Proteins remaining after the filtering process have low plasma concentrations and low molecular weight indicating they are enriched for EV derived proteins.

hemoglobin) were filtered out (**Figure 2C**). After the filtering process, 454 of the original 758 identified proteins remained (**Figure 2C**). EV-associated proteins were less abundant than contaminants (EV associated proteins: median=32ng/ml, interquartile range [IQR] = 7.0-180ng/ml; contaminants: median = 28µg/ml, IQR = 0.21-290µg/ml, p = 2.2e-16). Considering these characteristics, it is reasonable to hypothesize that the proteins with apex intensities within SEC fractions 17-19 are contained within a vesicle. It should be noted, however, that it may be possible for some proteins to be associated with both EVs and the EV-independent plasma proteome. In comparison to the co-migration based filtering, 686 of the 758 proteins were contained in the Exocarta database, suggesting that this peak filtering strategy is a more conservative, but more accurate strategy to distinguish between EV and contaminant proteins.

We evaluated the reproducibility of SEC separation using three replicate PPP samples processed using three different SEC columns. Each replicate PPP sample was processed with each SEC column, and individual 2ml fractions between 12-23 were collected. Each collected fraction was subjected to proteomics analysis, and protein SEC elution profiles were constructed to determine reproducibility of EV separation. In total, 85 of the ECT100 proteins were identified in each replicate, and their elution profiles were highly correlated both within the same SEC column and across SEC columns (**Figure 3A, B-C**). Furthermore, the 4 ECT100 protein identified as possible plasma contaminants above (A2M, FN1, THBS1, LGALS3BP) displayed reproducible shifts in elution differentiating them from all other ECT100 proteins (data not shown). We also assessed the reproducibility of exosome protein intensities using this replicate analysis. For this, we

summed the intensity of each protein observed in each sample across all six fractions of each SEC column. The median coefficient of variation (CV) of protein intensities was

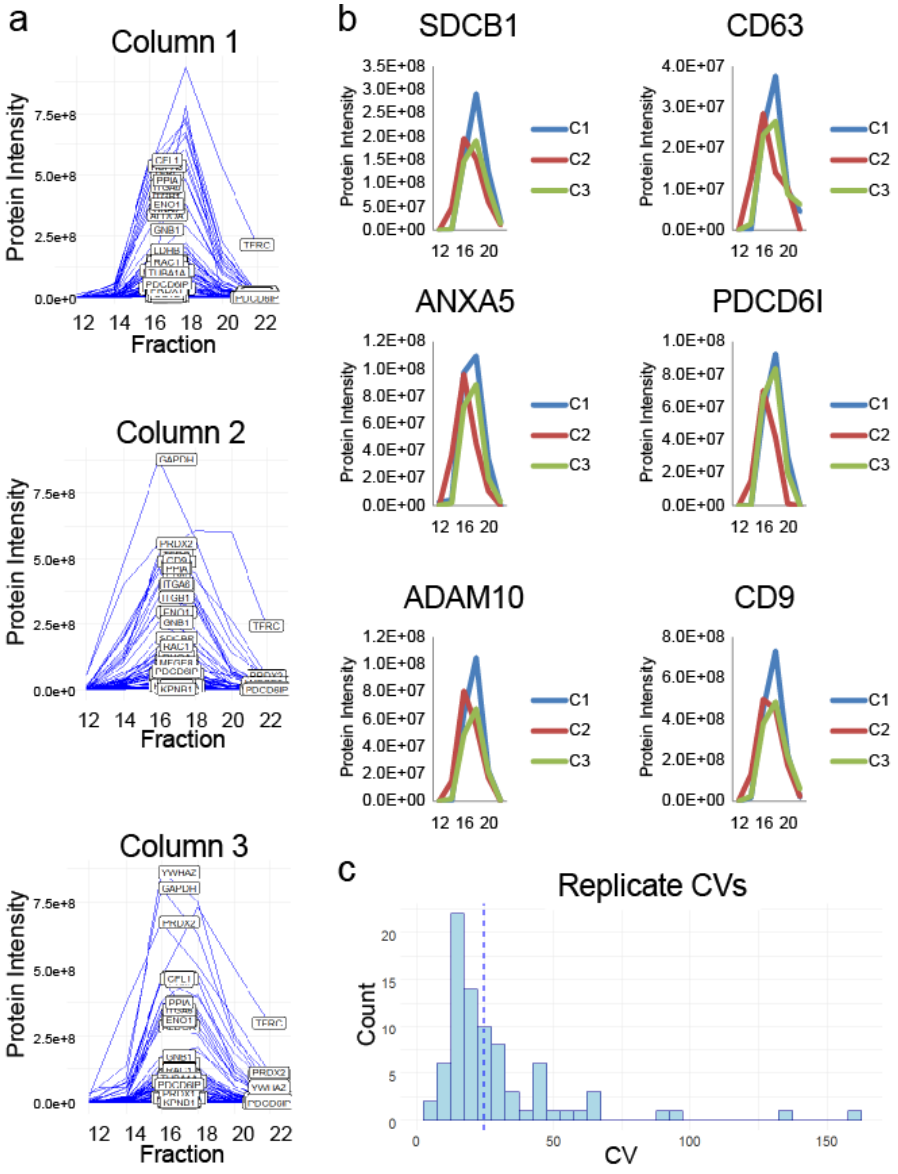

Figure 3. SEC Separation is reproducible across columns. Three separate SEC columns were used to analyze 3 replicate platelet poor plasma (PPP) samples collected in six individually processed fractions across the EV elution range. (A) 85 exocarta 100 (ETC100) proteins were identified in each replicate and elution profiles were highly correlated across each column. (B) Elution profiles for several commonly observed EV proteins are also highly correlated across columns. (C) CV's calculated from summed protein intensity of the 85 observed ETC100 proteins to illustrate the quantitative reproducibility of SEC separation.

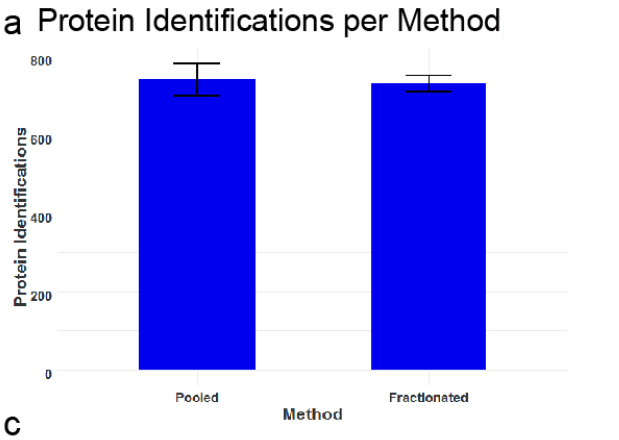

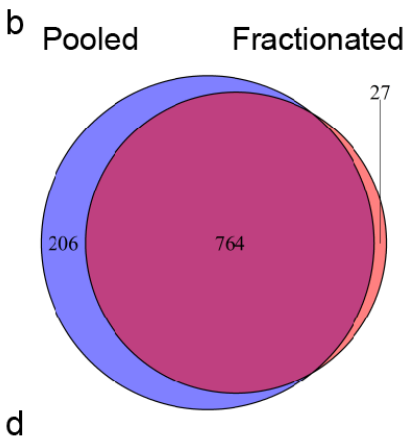

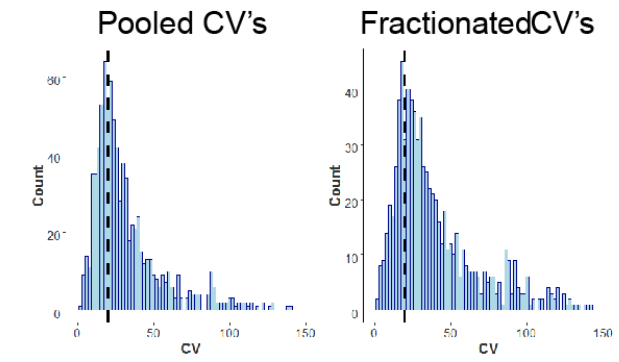

d

EV Marker Protein	Fractionated CV	Pooled CV
SDCBP	14.6	12.0
ADAM10	16.6	8.8
CD63	2.5	14.3
ACE	26.7	12.4
CD9	23.7	18.6
ANXA11	21.4	13.7
PDCD6IP	27.2	20.6
EHD4	25.5	23.7
Mean	19.8	15.5

Figure 4. Mass spectrometry analysis of unfractionated extracellular vesicles (EV's) and EV's fractionated by size exclusion chromatography (SEC) yield similar results. A reproducibility and performance comparison was performed for fractionated and unfractionated EV's. EV's were isolated from replicate plasma samples using three different SEC columns. (A) Bar chart displaying similar numbers of protein identifications resulting from unfractionated EV's (n=3) and EV's fractionated by SEC (n=3). (B) Venn diagram displaying the protein identification overlap observed between the unfractionated and fractionated EV's. (C) Coefficient of variation (CVs) calculated from the replicate measurements display comparable precision between the unfractionated and fractionated EV's. (D) Table displaying the CVs for several proteins commonly observed in EV's for each method.

20.89 (IQR 16.75-30.54), which is within the acceptable limits of typical label-free proteomics experiments (51-53).

Collecting and analyzing individual SEC fractions is labor intensive, error prone, and restricts sample throughput. To streamline SEC-based exosome analysis, we tested the feasibility of pooling the EV-containing SEC fractions together as one sample for subsequent proteomic analysis. For this, SEC fractions 14 to 21 obtained from three additional replicates of the above reproducibility experiment were pooled as a single EV sample for each replicate. We identified a similar number of proteins when analyzing pooled or individual SEC EV fractions (pooled: 800±46, fractions: 826±23; **Figure 4A**), with a majority (76%) of proteins identified by both types of sample analysis (**Figure 4B**). Importantly, the CV of protein intensities was slightly better when analyzing a pooled EV sample versus individual EV fractions of a single sample (**Figures 4C, 4D**). Taken together, these results indicate that EVs elute from SEC columns in a predictable and quantitatively reproducible manner that is amenable to downstream mass spectrometry analysis of pooled SEC fractions.

SEC-MS increases EV protein identifications and precision compared to ultracentrifugation. The performance of SEC-MS in isolating EVs for proteomic analysis was compared to the conventional ultracentrifugation (UTC) approach. EVs were isolated from pooled PPP acquired from healthy donors (n = 2) in the rested and fasted state using SEC and UTC. Five replicate measurements were performed. Nanoparticle tracking analysis showed similar particle size for both methods (SEC: 78 ± 12nm, UTC: 82 ± 14nm, P= 0.90). However, particle counts were higher for SEC compared to UTC (SEC: 1.49e10 ± 3.6e9, UTC: 2.05e7 ± 1.2e7, P= 0.0008; **Figure 5A, 5B**), indicating increased recovery

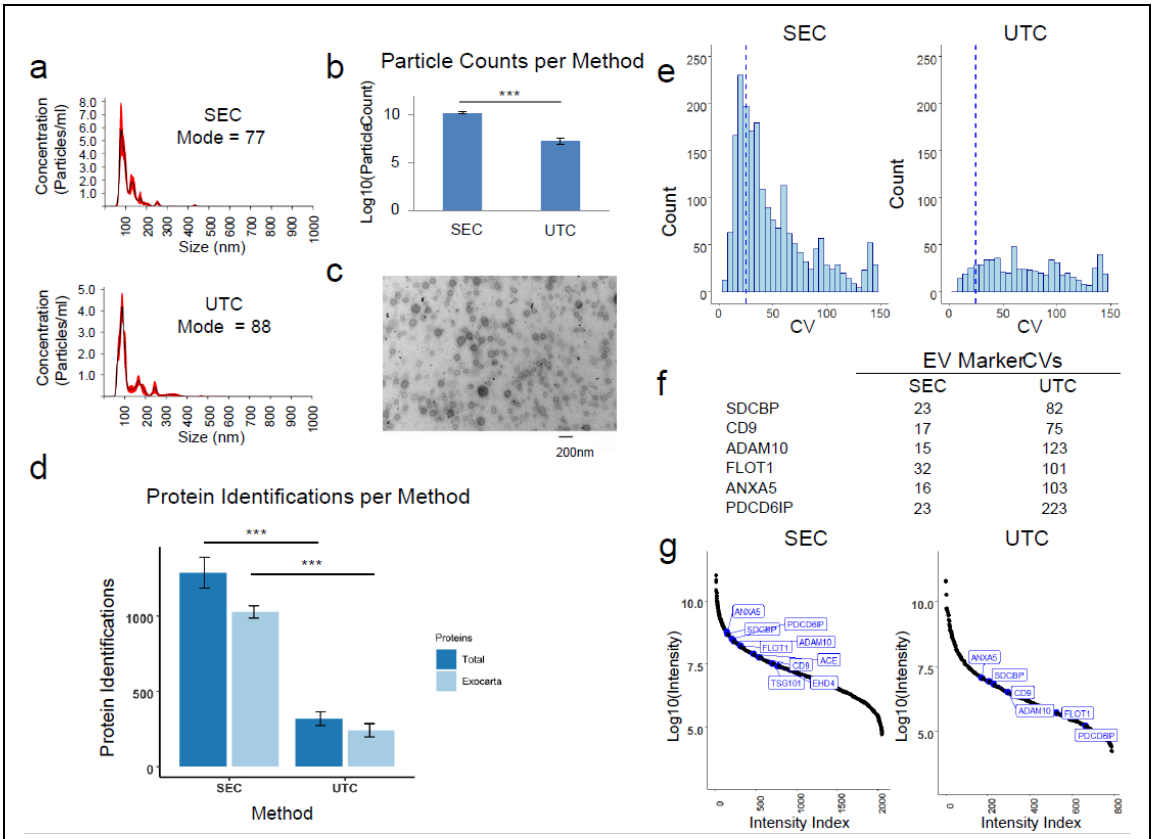

Figure 5. Comparison of extracellular vesicle protein identifications following size-exclusion chromatography and ultracentrifugation. Size distribution (A) and particle count (B) characterization of extracellular vesicles (EVs) isolated from platelet poor plasma (PPP) using size-exclusion chromatography (SEC) or ultracentrifugation (UTC) by nanoparticle tracking (NTA). (C) Transmission electron microscopy (TEM) image of EV isolated from plasma using SEC. (D) Experiments from five replicate analyses of pooled PPP showed that SEC produced approximately 3-fold more identifiable proteins compared to UTC. Dark blue bars represent the total number of protein identifications for each replicate, while light blue bars represent the number of the identified proteins which associate with the Exocarta database. (E) Histogram displaying the coefficient of variation (CV) calculated from protein intensity measurements of the five replicate measurements. In total, 562 proteins with a CV of less than 25% were identified with SEC, compared to just 73 with UTC. (G) CVs for several EV marker proteins identified by SEC and UTC. (F) Protein identifications from each method plotted as ranked abundance against log 10 intensity shows that SEC results in higher recovery of EV proteins relative to UTC.

of EVs with SEC compared to UTC. EVs isolated with SEC also appeared to be intact and have a diameter of less than 100nm by transmission electron microscopy (**Figure 5C**). Proteomics analysis revealed that SEC produced significantly more protein identifications than UTC (SEC: 1268 ± 102, UTC: 319±45, p= 2.6E-6) (**Figure 5D**). The CV of the

protein intensities obtained from SEC-MS was significantly lower than those obtained via UTC-MS (**Figure 5E**). In total, 562 proteins quantified by SEC-MS had CVs less than 25% when compared to only 73 proteins reaching this threshold for the UTC-MS. Moreover, CVs of canonical EV marker proteins were lower with SEC-MS when compared to UTC-MS (**Figure 5F**). A closer inspection of the canonical EV protein marker intensity data suggested that UTC-MS was either unable to detect these proteins or detected them with a lower intensity when compared with SEC-MS, which resulted in a higher CV for these proteins (**Figure 5G**). This is suggestive of suboptimal EV recovery with UTC, which was noted by others (31).

SEC-MS Measurements are Linear and Precise. SEC-MS outperformed the conventional UTC-MS approach for plasma-derived EV proteomic analysis. To test the quantitative performance of SEC-MS across a range of EV abundance, human plasma was serial-diluted with exosome-depleted bovine serum (EDBS). For this experiment, non-platelet depleted plasma was used (i.e., platelet rich plasma PRP), to extend the top end of the EV dynamic range. Five replicates of a dilution series (neat plasma, x2, x4, x8 and neat EDBS) were generated, and each dilution series replicate was processed using a separate SEC column. With this design, it was possible to simultaneously assess reproducibility across SEC columns and linearity of the dilution. More than 2,080 proteins were detected across the experiment, and 1,418 proteins remained after filtering out proteins that were indistinguishable from bovine proteins based on the observed peptide evidence. Protein intensities of multiple canonical EV proteins displayed linear curves across the dilution range (**Figure 6A**). A dilution curve analysis of the entire data set found 850 proteins with

an r^2>0.9 (**Figure 6B**), indicating high linearity across the quantitative range. Protein

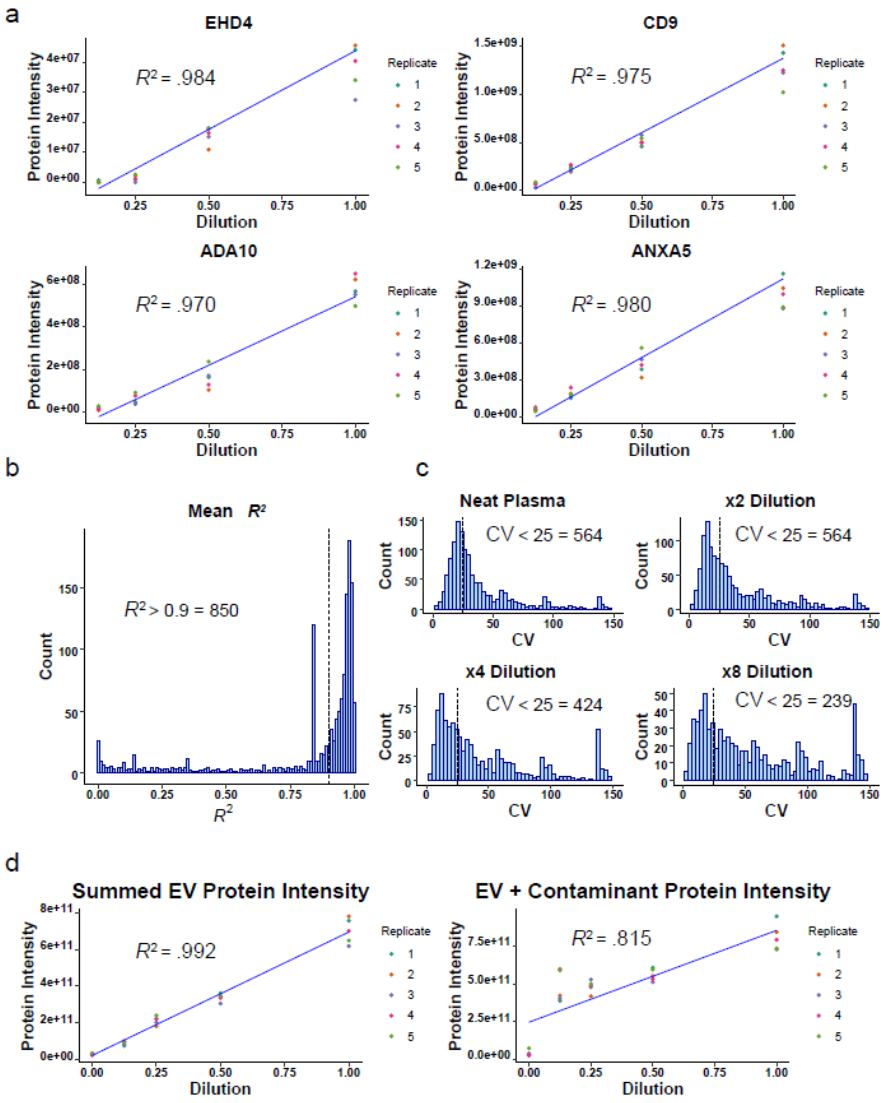

Figure 6. Evaluation of quantification performance in biological samples. (A) Pooled human plasma was serially diluted with exosome-depleted fetal bovine serum (EDFBS) and extracellular vesicles (EVs) were isolated from five replicates of each dilution level. Dilution curves fit with a linear regression are displayed for several select EV marker proteins. Average protein abundance values at each dilution point were used to fit the curve. (BC) Histogram representing mean R2 values of the replicate dilution curves for all identified proteins showed 850 proteins had an R2 value > 0.9. (CD) Analysis of the coefficients of variation (CVs) of the five replicate measurements at each dilution point showed low variation at each dilution point. (D) Linear regression showing the high correlation between summed EV protein intensity and dilution factor. Correlation is much higher when contaminants identified using the co-migration based filter process are removed prior to summing protein intensity (contaminants filtered; R2 = 0.992 vs no filtering; R2 = 0.815).

intensity precision of replicate measurements at each dilution point was also measured. This analysis identified 564, 564, 424 and 239 proteins with CVs less than 25% at the neat plasma, x2, x4 and x8 dilution points, respectively (**Figure 6C**). To test the potential for using total EV associated protein intensity as a measure of overall EV abundance, the total intensities of all EV associated proteins (i.e. proteins remaining after filtering contaminants identified by the co-migration based filtering process described above) observed in a sample was plotted against its dilution factor (**Figure 6D**). Summed EV associated protein intensity was highly correlated with the dilution factor ($r^2 = 0.992$), indicating that this approach may provide an accurate readout of total EV abundance. Plotting summed EV plus contaminant protein intensity for each sample against the dilution factor produced a lower r^2 of 0.815, reinforcing the notion that the co-migration based filtering process is useful for identifying contaminants.

EVs derived from different cell types contain both common and unique protein cargo. Cell culture-based EV experiments were performed to identify EV proteins that may be unique to specific EV-producing tissues (e.g., platelets, skeletal muscle, adipose, liver, leukocytes). EVs were isolated from media collected from cultured primary human myotubes, primary human adipocytes, Huh7 hepatocytes, leukocytes, and isolated human platelets, and their protein cargo was profiled using SEC-MS. Many identified EV proteins were common to all cell types, but a large number of putative cell-specific EV proteins were also identified **(Figure 7A).** A total of 118, 310, 350, 180 and 121 unique proteins were identified in platelet, leukocyte, myotube, hepatocyte, and adipocyte EVs,

a

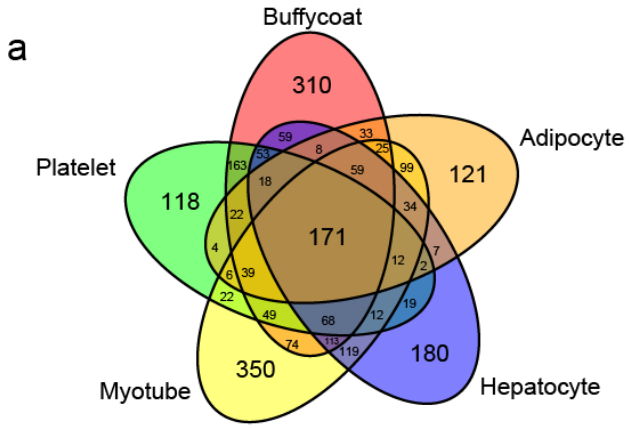

b

Cell Type	Gene Set Description	Size	Expect	Ratio	P-Value	FDR
Adipocyte	extracellular structure organization	400	2.7	7.4	2.2E-12	2.0E-08
	keratan sulfate catabolic process	12	0.1	74.4	7.2E-11	3.3E-07
	aminoglycan catabolic process	65	0.4	20.6	4.7E-10	1.1E-06
	proteolysis	1731	11.6	2.8	1.8E-08	2.5E-05
Hepatocyte	intracellular transport	1803	18.4	2.4	2.4E-08	8.3E-05
	endomembrane system organization	400	4.1	4.7	2.8E-08	8.3E-05
	DNA replication initiation	32	0.3	18.4	7.5E-07	1.2E-03
Leukocyte	cell activation	1335	21.8	4.3	<2.2E-12	<2.2E-12
	immune effector process	1141	18.6	5.2	<2.2E-12	<2.2E-12
	exocytosis	894	14.6	5.5	<2.2E-12	<2.2E-12
Platelet	regulated exocytosis	783	4.9	3.6	1.7E-06	4.8E-03
	blood coagulation	322	2.0	5.4	5.9E-06	6.8E-03
Myotube	muscle structure development	610	11.5	4.8	<2.2E-12	<2.2E-12
	actin filament-based movement	132	2.5	11.2	<2.2E-12	<2.2E-12

Figure 7. Comparison of EV protein content from different cell types. (A) Venn diagram showing the protein composition overlap of extracellular vesicles (EVs) isolated from primary human myotube, primary human adipocyte, HUH7 hepatocyte, platelet and leukocyte conditioned medium (CM). While many of the identified proteins were common to several cell types, some were unique to each. (B) Over representation enrichment analysis (ORA) of proteins identified uniquely in each cell type identified gene sets associated with each respective tissue.

respectively. Gene ontology (GO) overrepresentation enrichment analysis (ORA) of putative cell-type specific EV proteins revealed several distinct gene sets including actin filament-based movement and muscle structure development (myotube), proteolysis (adipocyte), intracellular transport (hepatocyte), blood coagulation (platelet), and immune effector process (Leukocyte) (**Figure 7B**). Putative cell-specific EV proteins were merged with tissue specific proteins from The Human Protein Atlas (HPA) (54). Prior to merging putative cell-specific EV proteins with HPA data, proteins which were unique to the

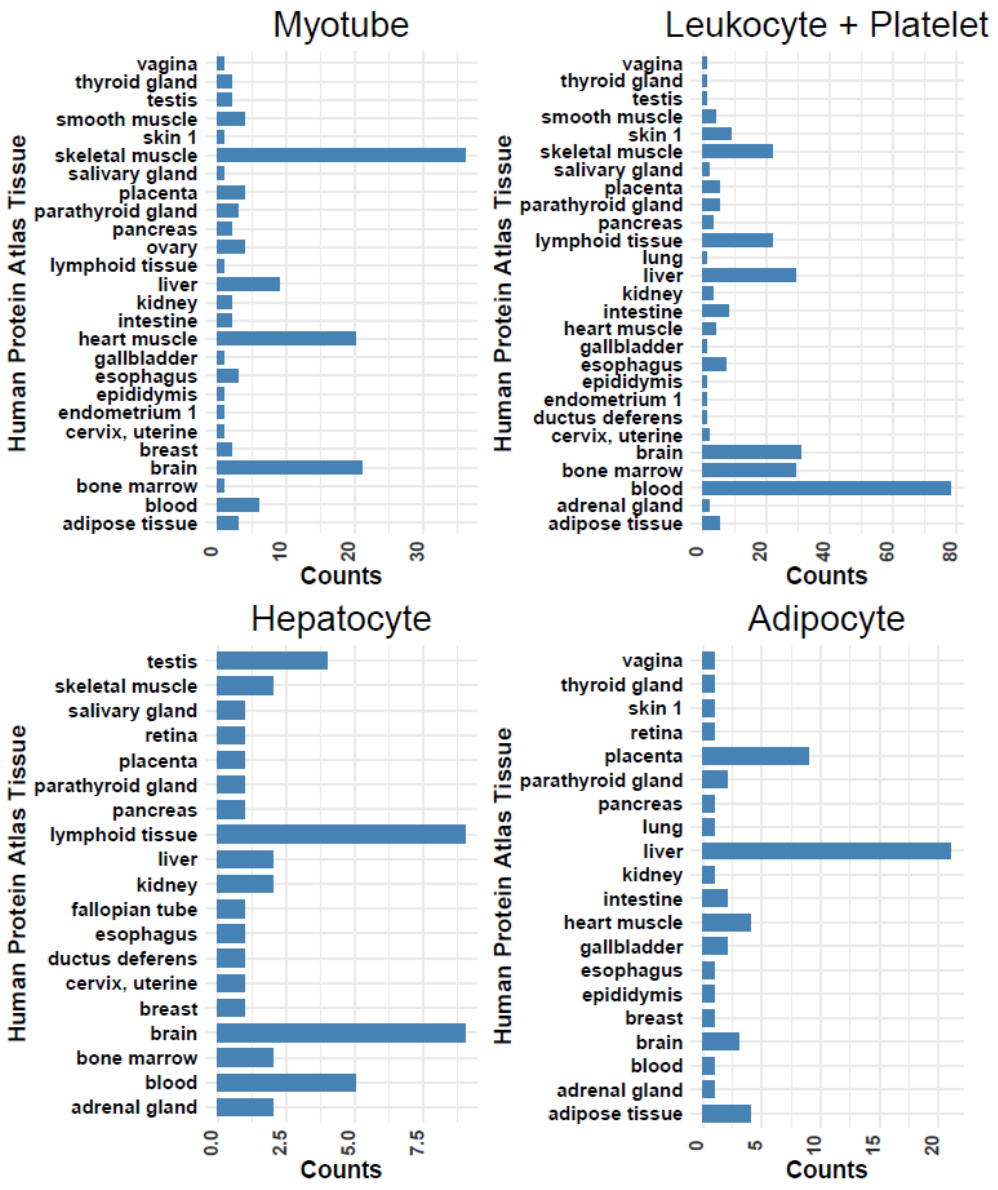

Figure 8. Bar plots illustrating the agreement between Human Protein Atlas tissue specific data and putative cell-line specific EV data from the current study. Each bar plot illustrates tissue specificity according to the Human Protein Atlas for all identified putative cell-specific EV proteins.

combined list of platelet plus leukocyte EVs (platelet + leukocyte specific proteins) were determined because HPA considers "blood" as one tissue. HPA "tissue enhanced" and "tissue enriched" data aligned with 67 myotube ("muscle" in HPA) and 120 platelet +

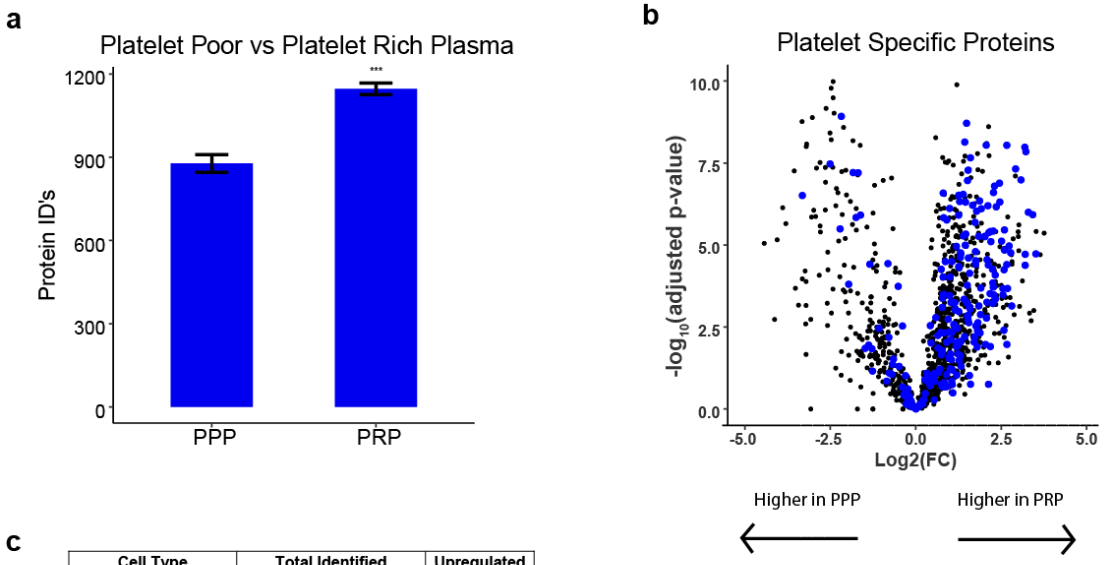

c

Cell Type	Total Identified	Upregulated
Multiple Cells	526	158
Platelet + Leukocyte	308	124
Unknown	477	52
All Cells	187	45
Myotubue	53	13
Hepatocyte	31	7
Adipocyte	36	1

Figure 9. Differential comparison of extracellular vesicle proteins derived from platelet poor and platelet rich plasma. (A) Mass spectrometry analysis of extracellular vesicles (EVs) isolated from six replicates of pooled platelet-poor plasma (PPP) or platelet-rich plasma (PRP) showed significantly increased protein identifications in PRP. (B) Volcano plot representing the relative difference in protein abundance between PPP and PRP. Proteins identified only in EV's derived from isolated platelets or leukocytes are colored in blue to show illustrate the overwhelming increase in abundance of platelet and leukocyte derived EVs in PRP plasma. (C) Table showing the number of identified and upregulated proteins form each cell type.

leukocyte ("blood" or "lymphoid" in HPA) specific proteins EV proteins, whereas only 4 adipocyte ("adipose" in HPA) and hepatocyte ("liver" in HPA) putative cell-specific EV proteins each agreed with HPA data (**Figure 8**). These data are a valuable resource in efforts to track the composition and origin of circulating EVs.

Platelet and leukocyte derived EVs are abundant in plasma and can be released *ex vivo*. *Ex vivo* platelet activation is a well characterized phenomenon with implications in

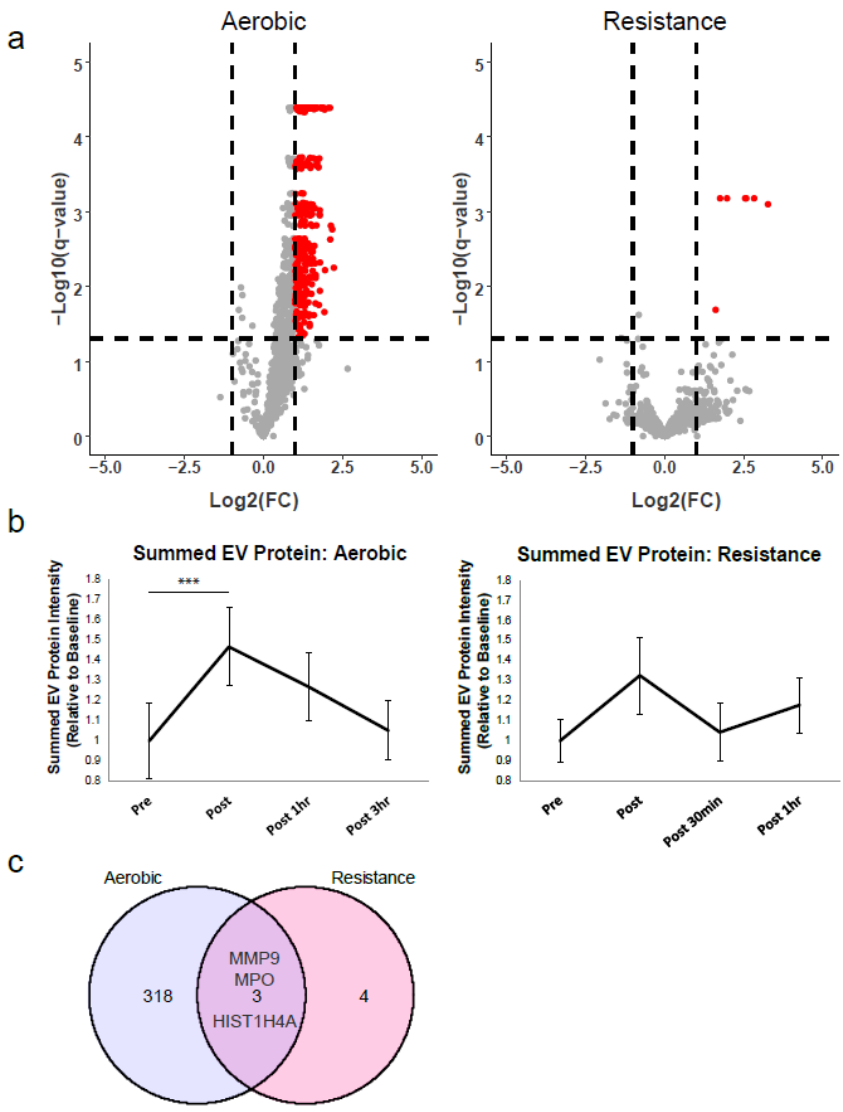

Figure 10. Aerobic exercise triggers an increase in extracellular vesicle protein abundance. (A) Volcano plots showing the increase in EV-associated protein abundance immediately after exercise for aerobic and resistance exercise. (B) Summed EV-associated protein intensity normalized to pre-exercise is displayed for aerobic and resistance exercise. Summed EV-associated protein is significantly increased after exercise (p= 0.0006) and returns to pre exercise levels by 3hr. (C) Venn diagram showing common and uniquely regulated proteins for aerobic and resistance exercise.

transfusion medicine and blood processing. Several fold increases in platelet derived EVs have been observed following freeze-thaw of standard plasma (i.e., platelet rich plasma; PRP) (40,41). Obtaining unfrozen plasma to avoid platelet EV release prior to EV analysis

is logistically difficult for human studies. Hence, it is important to assess the effect of platelet depletion on SEC-MS toward the goal of making SEC-MS compatible with frozen plasma samples. Blood was collected from two healthy volunteers, pooled, and divided to be prepared as PPP or PRP. EVs were isolated and analyzed from six replicate samples of each preparation type using SEC-MS. As expected, the average number of protein identifications was significantly higher in the PRP relative to the PPP (PRP = 1147 ± 20, PPP = 877 ± 32, p = 6.0E-8) (**Figure 9A**). Furthermore, the abundance of platelet + leukocyte specific proteins were significantly higher in the standard plasma compared to PPP (**Figure 9B**). In total, 308 platelet + leukocyte specific proteins were identified in the PPP vs PRP comparison. Of these, 124 were significantly increased in PRP relative to PPP > log2FC of 1.0. These results provide evidence that platelet and leukocyte-derived EVs released *ex vivo* account for a majority of the increased EV proteins observed in standard plasma (i.e., PRP).

Acute exercise triggers EV release. We applied the SEC-MS method to evaluate the effect of acute exercise as a physiological stimulus on plasma EV proteome cargo in humans. The effects of exercise on EV release into circulation has been investigated by others (7,55), and we considered acute exercise as an appropriate physiological intervention to determine the ability of the approach to detect the EV proteome changes.

Although the objective was not to compare and contrast with the previous reports, we wanted to determine whether the current PPP-SEC-MS approach with its methodological innovations allow the detection of similar or larger number of proteins

from human EVs released following exercise. Moreover, we also sought to identify the specific cellular origin of many EV proteins. We determined the differential responses of EV protein abundance following one bout of acute high intensity aerobic (aerobic: n = 14) and a moderate bout of single leg resistance exercise (resistance: n = 16) (Supplement table 7).

Fourteen healthy individuals performed a single bout of aerobic exercise at ~90% of VO_2 peak (56), and samples were collected before exercise (pre), within 10 min (immediately-post), 1hr (post-1hr), and 3hr (post-3hr) following exercise. Sixteen

Term	Count	PValue	Fold Enrichment	FDR
Biocarta: mPRPathway:How Progesterone Initiates the Oocyte Maturation	17	3.02E-08	4.865269	6.55E-06
Biocarta: salmonellaPathway:How does salmonella hijack a cell	10	4.93E-07	7.48503	5.35E-05
Biocarta: uCalpainPathway:uCalpain and friends in Cell spread	11	9.87E-07	6.296231	7.14E-05
Biocarta: actinYPathway:Y branching of actin filaments	12	1.31E-06	5.560308	7.10E-05
Biocarta: rhoPathway:Rho cell motility signaling pathway	15	1.78E-06	4.292885	7.74E-05
Biocarta: cskPathway:Activation of Csk by cAMP-dependent Protein Kinase Inhibits Signaling through the T Cell Receptor	12	2.39E-06	5.307567	8.64E-05
Biocarta: integrinPathway:Integrin Signaling Pathway	15	5.93E-06	3.944813	1.84E-04
Biocarta: cdc42racPathway:Role of PI3K subunit p85 in regulation of Actin Organization and Cell Migration	10	5.99E-06	6.081587	1.63E-04
Biocarta: monocytePathway:Monocyte and its Surface Molecules	8	2.38E-05	7.076756	5.75E-04
Biocarta: neutrophilPathway:Neutrophil and Its Surface Molecules	7	2.46E-05	8.514222	5.33E-04
Biocarta: lymphocytePathway:Adhesion Molecules on Lymphocyte	7	6.75E-05	7.568197	0.00133
Biocarta: mCalpainPathway:mCalpain and friends in Cell motility	10	1.51E-04	4.422972	0.002726

Table 1. Related to figure 11. Significantly enriched functional annotations after aerobic exercise using. Annotations were obtained using the DAVID functional enrichment tool.

additional individuals performed a single bout of unilateral knee extensor resistance exercise consisting of 3 sets of 10 repetitions at 70% of their 1-repetition maximum (1RM) (Robinson et al., 2017). Each participant's 1RM was determined at least 7 days, but no more than 30 days prior to the study visit. Samples were collected before (pre), within 10 min (immediately-post), 30min post (post-30min) and 60 min (post-60min) following exercise. All samples were analyzed by PPP-SEC-MS. We identified 2736 proteins in the aerobic exercise group (**Figure 10A**). Time course analysis of the response to aerobic exercise utilizing summed EV associated protein intensity showed a significant increase in circulating EV protein abundance immediately following aerobic exercise ($p=0.0006$), which returned to pre-training levels by 3hr post-exercise (**Figure 10B**). Notably, a similar trend was observed in ADAM10 positive particles measured by nano-flow cytometry (nFLC) immediately after training ($p=0.055$; data not shown). Conventional nanoparticle tracking analysis (data not shown) did not reveal the same post-exercise increase in particle count as summed EV protein intensity of nFLC. This suggests that SEC-MS and nFLC are more sensitive methods for detecting shifts in EV abundance with exercise compared to particle counting. The immediately-post aerobic exercise time-point revealed an increase in the abundance of 321 EV-associated proteins (**Figure 10A**). Functional enrichment analysis of these proteins indicated that they are central to CDC42 mediated cell migration, integrin signaling and immune function as indicated by enrichment of lymphocyte adhesion molecules, monocyte surface molecules and regulation of T-cell activation (Table 1). Similarly, Ingenuity Pathway Analysis (IPA) showed that these proteins were enriched for additional immune regulation processes such as leukocyte extravasation and CXCR4

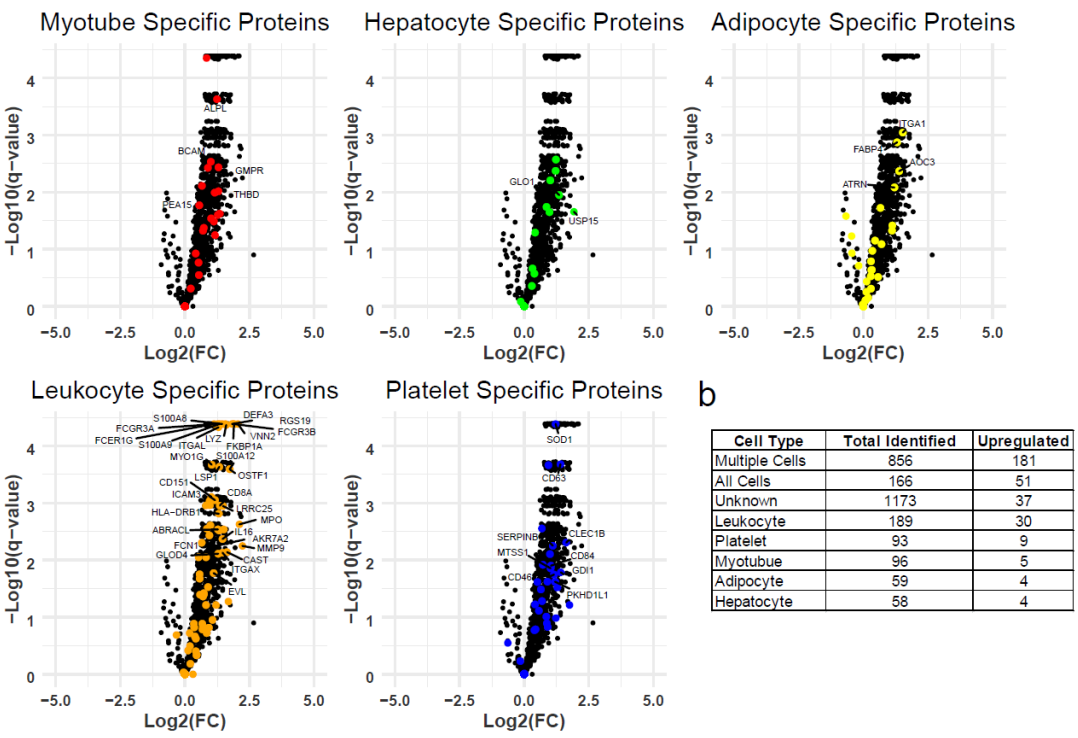

Cell Type	Total Identified	Upregulated
Multiple Cells	856	181
All Cells	166	51
Unknown	1173	37
Leukocyte	189	30
Platelet	93	9
Myotubue	96	5
Adipocyte	59	4
Hepatocyte	58	4

Figure 11. Cell specific EV proteins are upregulated after aerobic exercise. (A) Volcano plot illustrating the increase in EV protein abundance after aerobic exercise. Proteins identified uniquely from each cell type (Figure 5) are highlighted in individual volcano plots and significantly upregulated proteins (log2FC > 0.5) are labeled. (B) Table showing the number of identified and upregulated proteins form each cell type. The highest number of cell type specific proteins were found to be from leukocytes and platelets.

signaling. Additional pathways including glycolysis and signaling via Rho GTPase, IL-8, and integrin were also differentially regulated by exercise (data not shown). We next overlaid these data with the cell-type specific EV data we generated previously (**Figure 7A**) to assess the source of circulating EV proteins. When using cell type-specific EV proteins, we found proteins specific to myotubes (96), hepatocytes (58), adipocytes (59), leukocytes (189), and platelets (93) (**Figure 11A**). Interestingly, at the immediate post

exercise time point we found significantly upregulated proteins that were specific to each cell type profiled, including 30 leukocyte EV-specific and 5 myotube EV-specific proteins, of which 19 and 3 were supported by HPA tissue specific data respectively, demonstrating that EVs from different tissues can be measured in the plasma circulation. Collectively, these data highlight that one session of high intensity aerobic exercise leads to robust changes in circulating EV protein abundance, which may play an important role in regulating the metabolic and immune responses of training.

The samples of from the single leg resistance exercise analysis identified 3138 total proteins. EV-associated protein intensity displayed an upward trend post exercise, however, this increase failed to reach significance ($p = 0.17$) (**Figure 10B**). Analysis of the post resistance exercise time point found only 7 proteins which significantly were upregulated and 1 protein which was down-regulated, in stark contrast to the robust increase of EV proteins triggered by the acute bout of aerobic exercise (**Figure 10A**). Of the 7 upregulated proteins, 3 were commonly upregulated by the aerobic exercise bout (**Figure 10C**). Interestingly, 2 of the 3 commonly upregulated proteins were found to be specific to leukocytes in our cell type specific experiments further implicating immune modulation in response to different modes and intensities of exercise. Among the upregulated proteins common to both exercise responses was MMP9 (Matrix metallopeptidase 9) which is involved in functions that include neutrophil action, angiogenesis and wound healing.

Discussion

Here we describe an optimized SEC-MS method for proteomic analysis of plasma EVs that offers superior quantitative performance and reproducibility compared to conventional EV analytical approaches. Importantly, this SEC-MS method exhibited linearity over a biologically relevant dynamic range and is sensitive to small differences in protein abundance. Additionally, the orthogonal separation of EVs and plasma protein contaminants provided by the SEC column was leveraged to filter contaminants from plasma proteins within the EV proteome. Using SEC-MS, we demonstrate the importance of using PPP to avoid the confounding effects of *ex vivo* release of platelet EVs. After benchmarking quantitative performance of SEC-MS, we used the method to demonstrate the time-related effects of two different modes and intensities acute exercise bouts on changes in plasma EV protein abundance

The proteomic depth of plasma EVs isolated with UTC or commercially available kits is limited by factors including plasma protein contamination and low EV recovery (**Figure 1**). We show that SEC purification of EVs followed by proteomic analysis substantially mitigates plasma protein contamination. Particle counts, EV protein intensities, and EV protein identifications were markedly higher when plasma EVs were isolated with SEC compared to UTC (**Figure 5A-B, D**). Further, the precision of replicate SEC-MS measures is far superior to that based of UTC-MS; capable of quantifying >500 proteins with CV less than 25% (**Figure 5E**).

Beyond demonstrating utility of SEC for isolating EVs, we also present a strategy, based on the fractionation properties of SEC, to distinguish EV-associated proteins from plasma protein contaminants based on their elution patterns (**Figure 2C**). This process

relies on identification of proteins that co-elute with known EV proteins, allowing us to reproducibly identify four proteins in the ECT100 as likely plasma protein contaminants, rather than EV derived proteins. However, we cannot categorically exclude the possibility that some proteins may be commonly present in both EVs and plasma proteome. Nevertheless, the SEC-MS method can discern if the majority of the protein abundance in a sample is derived from plasma contaminants or EVs. This is particularly useful because accurate EV abundance measurements are obtained by filtering contaminants and summing EV-associated protein intensities (**Figure 6C**). Additionally, SEC-MS can also be used to validate whether a candidate protein is derived from EV, with an added advantage of being applicable for any EV protein and not limited to EV membrane proteins. There are previous reports (7,39) of the relative quantification of plasma EV proteome. However, the quantitative performance of those methods has not been described. We benchmarked the quantitative performance of SEC-MS to validate it for relative quantification of EV associated proteins in biological samples. Using a dilution series experiment, we show that over 850 EV proteins can be measured from human plasma with an $r^2 > 0.9$. We also observed low quantitative CVs at multiple dilution points indicating high precision. *Ex vivo* activation of platelets is known to cause a massive release of EVs, resulting in sample contamination and confounding results. To avoid this issue, ISEV and ISTH guidelines recommend including a platelet depletion step prior to refrigerating plasma. Although this step is strongly recommended and widely recognized by the EV research community, several recent studies examining the plasma EV proteome have utilized frozen serum or plasma without platelet depletion (7,39,57,58) which facilitates analysis of samples from

well characterized previous studies. In order to assess the extent of platelet-derived EVs released during sample processing, we performed a differential analysis on pooled plasma with and without platelet depletion using SEC-MS. The detected proteins were also cross-referenced with platelet + leukocyte specific EVs derived from the cell culture-based EV experiment. This analysis showed large increases in platelet and leukocyte specific EV protein identifications and abundances in non-platelet depleted plasma relative to PPP. These results highlight the importance of the platelet depletion step to avoid sample contamination and confounding results. This study demonstrates that the SEC-MS offers an opportunity to analyze the PPP EV proteome, which contains fewer EVs but more accurately reflects the composition of circulating EVs.

We applied SEC-MS to characterize the acute effects of a single bout of high intensity aerobic exercise or resistance exercise on plasma EV proteome. We identified 3409 proteins in this experiment using a short 1hr MS method; substantially shorter than UTC-MS methods described previously (7). In the present study, >300 proteins were significantly increased following a single bout of aerobic exercise. We also noted that acute single-leg resistance exercise bout increased only 7 EV proteins although three of them are common to both exercise modes. Increased cardiac output and more dynamic nature and high intensity (90% of VO_2peak) of aerobic exercise is a likely reason for the substantially more robust response to aerobic exercise in comparison with the response to the modest one-leg resistance exercise. Although the goal of this exercise was not to contrast the effects of exercise modality on circulating EV cargo, it is interesting to note that some modest changes in EV proteomic cargo could be detected even following a low-

intensity, short duration bout of single leg resistance exercise. We also performed cell culture-based EV profiling experiments and identified candidate tissue-specific proteins that are released immediately after an aerobic exercise bout. Although skeletal muscle contributed to the circulating EV pool, it is of great interest that EV proteins specific to other tissues including leukocytes were dominant following a bout of aerobic exercise and linked these proteins with important functions including signaling, immunological response, repair and angiogenesis. How aerobic exercise interacts with other tissues, especially leukocytes, remains to be determined. It has been shown that exercise-induced muscle tissue damage attracts many circulating cells, including those involved in immunological reactions that remove degraded proteins and stimulate protein synthesis (59). It appears that acute exercise stimulates these circulating cells to release proteins via EVs which may enable the transport of important signals to multiple organs. It remains to be determined whether these signals contribute to the exercise responses in remote organs such as liver and brain. Also, the exact mechanism of exercise-mediated EV release from liver, adipocytes and platelets also remain to be determined.

In summary, our study describes the development and quantitative performance of a reproducible SEC-MS assay for plasma EV protein analysis. We demonstrate that this assay yields deeper proteomic coverage and higher precision when compared to more commonly used approaches, especially UTC-MS. Our study makes an important advance in the quest to determine the tissues of origin of EVs found in circulation. We demonstrate the importance of platelet poor plasma to avoid *ex vivo* contamination from platelet derived EVs. We also describe an approach to filter plasma protein contamination even after SEC-

based exosome isolation. We benchmarked the quantitative performance of SEC-MS and demonstrate that it can be usefully employed in human clinical studies. Finally, we demonstrated the EV proteome response to acute bouts of exercise, and future studies will be needed to determine the effects of exercise intensity, duration, and modality on the molecular cargo of circulating EVs in humans.

Methods

Study overview

This study was approved by the Mayo Clinic Institutional Review Board and conducted in accordance with the Declaration of Helsinki. For method development and analytical validation, blood was collected from a group of volunteers composed of both males and females. For the high intensity aerobic exercise study seven male and seven female subjects were recruited. For the resistance exercise study eight male and eight female subjects were recruited. Subject characteristics are summarized in Table S7.

Measurement of $VO_{2\ max}$.

VO_{2max} was measured with indirect calorimetry (Medgraphics Diagnostics) using an electronically braked cycle ergometer (Lode Medical Technologies). VO_{2max} was defined as reaching a perceived exertion > 17 on the Borg RPE scale with an RER > 1.1 (mean ± SD [Range]: 1.17 ± 0.02 [1.15–1.19]), and achieving a heart rate within 10% of the age-predicted maximal heart rate.

High intensity aerobic exercise

Subjects completed one bout of high intensity cycling (4 bouts of 4 min at > 90% of VO_{2max} with 3 min pedaling at no load between bouts), as previously described (56).

Acute resistance exercise

Subjects completed one bout of one-legged knee extension exercise (3 sets of 10 repetitions at 70% of 1-repetition-maximum, with 1min rest in-between sets).

Cell culture

Human skeletal muscle myoblasts (HSMM) were purchased from Lonza and grown in skeletal muscle cell growth medium (Cell Applications, cat# 151K-500). Media was changed three times a week until he cells reached 70% confluency at which point they were differentiated to myotubes in Dulbecco's Modified Eagle Medium/F-12 (DMEM/F-12) containing penicillin(100 U/mL), streptomycin(100 ug/mL) and 2% horse serum. After differentiation the cells washed twice with PBS and were placed back into growth medium supplemented with 2% exosome depleted bovine serum (EDBS,Gibco,cat# A2720801). After 24hours the media was harvested and frozen.

Human pre adipocytes were cultured in preadipocyte growth medium-2 (PGM-2 Bullekit, Lonza cat# PT-8002) and the media was changed 2-3 times a week until the cells reached 80-90% confluency. The preadipocytes were differentiated to adipocytes according to the manufactures instructions. Once differentiated, the cells were washed twice with PBS and the media was replaced with PGM-2 prepared with 10% EDBS

(Gibco,cat# A2720801) and cultured for an additional 24hrs before the media was collected and frozen.

Isolated platelets were obtained from the Mayo Clinic blood bank. Platelet EVs were prepared as previously described (60). Briefly, the isolated platelets were washed with 3x in Tyrode-HEPES buffer (145mM NaCl, 2.9 mM KCl, 10mM HEPES, 1mM $MgCl_2$, 5mM glucose, pH 7.3) and re-suspended at a concentration of $6X10^8$/ml. Platelets were activated with thrombin (0.1U/ml) and incubated at 37°C for 30min with rotation every 10min. Platelets were then pelleted by centrifugation at 3200x g for 10min and the supernatant was collected and frozen at -80°C.

Huh7 hepatocytes were cultured in DMEM containing glucose(4.5 g/L) penicillin(100 U/mL), streptomycin(100 ug/mL) and 10% fetal bovine serum (FBS). Cells were grown to 90% confluency on 150mm tissue culture dishes. Cells were washed twice with PBS and then cultured for an additional 24hr in growth medium supplemented with 5% extracellular vesicle-depleted FBS, which was prepared by overnight centrifugation at 100,000g at 4C and 1% bovine serum albumin.

Human leukocytes were isolated from blood donated by two donors. Whole blood was drawn into 10-ml ETDA tubes and placed on the benchtop for 15minutes. After 15minutes each tube was centrifuged at 2,000xg for 10min at room temperature (RT) to pellet red blood cells. The buffy coat was isolated from 10 blood collection tubes and transferred to a 50ml Falcon tube. Cells were then re-suspended in 25ml of PBS, pelleted at 2,000xg and transferred to a new tube 3x to remove as many red blood cells as possible. The isolated leukocytes were then re-suspended in 25ml of PBS and pelleted them at

800rpm. The supernatant was then removed and this process was repeated 3x to remove platelets. Isolated leukocytes were then re-suspended in 10ml of PBS and placed on ice for 1.5hr. The supernatant containing the EVs was then collected for further processing.

EV isolation from cell culture media

Myotube, adipocyte, hepatocyte, platelet and leukocyte conditioned media were centrifuged at 2,000xg for 10 minutes to pellet cell debris. The media was then transferred to a new tube and centrifuged at 10,000xg for 20min to pellet large vesicles. The media was then filtered through a 0.2µm filter. Myotube, adipocyte, hepatocyte and platelet media were transferred to a 70-ml 100kD Centricon® Plus-70m filter unit to concentrate the media as previously described (61). The concentrated media was then diluted up to 2ml at which point the EVs were isolated using a qEV2.0 (Izon) size exclusion chromatography column and processed as described from plasma EVs. Leukocyte and red blood cell EVs were processed by ultracentrifugation UTC. Briefly, samples were pelleted at 10,000 x g to pellet large vesicles. The supernatant was transferred to a new tube and centrifuged at 100,000 x g for 1.5hr and digested as described for plasma EVs.

Blood collection and plasma preparation

Whole blood was drawn into ETDA tubes and placed on the benchtop for 15minutes. After 15minutes each tube was centrifuged at 2,000xg for 10min at room temperature (RT) to pellet red blood cells. The upper plasma fraction was then collected, transferred to a new sterile tube, and centrifuged again at RT for 10min at 2000xg. Platelet

poor plasma was isolated by carefully transferring the top layer of plasma to a new tube and then frozen at -80°C in 1ml aliquots.

Isolation of plasma extracellular vesicles by size exclusion chromatography (SEC)

Frozen platelet poor plasma was removed from the freezer, thawed on ice and centrifuged at 2,000xg for 10 min to pellet debris. The plasma was then transferred to a new microcentrifuge tube and centrifuged at 10,000xg for 10min to pellet larger vesicles. Following centrifugation the plasma was transferred to a new tube and placed on ice until analysis. Extracellular vesicle isolation was performed using a qEV 2.0 size exclusion chromatography column (Izon Science, Christchurch, New Zealand) following the manufactures protocol. Briefly, SEC columns were equilibrated to room temperature and flushed with 90ml of phosphate buffered saline (PBS) before use. Platelet poor plasma (time course analysis: 1.2ml, all other experiments: 2.0ml) was transferred into the sample loading reservoir of the SEC column. The column cap was then removed and the plasma sample was allowed to completely enter the column, at which point the sample loading reservoir was filled with PBS. The first 13ml of PBS fraction was discarded and the following 8ml's of EV containing fraction were collected for each sample. The SEC columns were then flushed with 90ml of PBS before the addition of the next sample. The 8ml of EV containing fraction for each sample was then pelleted by ultracentrifugation at 100,000xg for 1.5hr at 4°C. Following ultracentrifugation the supernatant was discarded and all residual PBS was removed before tryptic digestion.

Nano-particle tracking analysis (NTA) and transmission electron microscopy (TEM)

EVs isolated by SEC were measured by NTA using a 10 fold dilution of the SEC column eluate. EVs isolated by UTC were re-suspended in PBS prior to measurement. All NTA measurements were obtained using a Nano-sight LM10-HS with a 532nm laser running on NTA software v3.2. Samples were diluted until they reached the manufacturers recommended concentration of 20-60 particles per frame and data was acquired in 3 x 60sec videos with a viscosity of 0.985-0.897cP, cameral level 13, detection threshold 2 and temperature of 25°C. For TEM, a 1ml volume of SEC column eluate was fixed with 16% paraformaldehyde (4% final). The sample (5µl) was deposited on formvar-carbon-coated nickel grid (150 mes), air dried for 15min, washed 6x with PBS, fixed in 1% glutaraldehyde/PBS for 5min and then washed 6x for 2min with stilled water drops. The grid was then transferred to a drop mixture of 4% uranyl acetate and 2% methycellulose (in a 1:9 ratio) for 5min. A paper filter was then used to remove excess solution and the sample was air dried for 1hr prior to observation with a JEOL (Peabody, MA) 1400 electron microscope at 80 KV.

Protein digestion and label free mass spectrometry analysis

Samples were processed in three separate batches. For the first batch, EV pellets were lysed with the addition of 50µl 0.04% ProteaseMax Surfactant (Promega, Madison WI) in 50mM Tris buffer pH 8.2 and vortexed for 1min. 5ul of 110mM DTT (5mM final) was then added to reduce disulfide bonds and the samples were heated at 70°C for 10min. Samples were then equilibrated back to room temperature over 20 minutes before

alkylation with 5µl 120mM IAA (10mM final) and incubated for 30min protected from light. Following alkylation an additional 0.675µl of 1.0% ProteaseMax was added prior to the addition of 0.1µg of Trypsin LysC mix. The samples were then vortexed and incubated at 37°C for 16hr. Finally, the digestion was terminated by adding 5µl of 5.25% TFA. Sample batches two and three were processed with an optimized method to yield deeper proteome coverage. For these samples, EV pellets were precipitated with the addition of 50µl of methanol. The methanol was then evaporated in a SpeedVac (Thermo Scientific, Waltham MA) and protein was reconstituted with 50µl of 50mM Tris pH 8.2 containing 0.002% zwittergent Z3-16 (EMD Millipore, Burlington MA) and subsequently heated at 95°C for 10min. All additional steps are the same as described above except ProteaseMax wan not added before the digestion.

LC-MS conditions

Digested samples (15µl) were loaded onto a 0.33µl OptiPak trap column (Optimize Technologies) packed with Halo C18 peptide ES stationary phase. The trap was then washed with an aqueous loading buffer composed of 0.2% FA and 0.05% TFA for 4 minutes at 10µl/min. After the wash, the 10-port valve was switched and peptides were flushed off of the trap onto a 25cm x 75µm PicoFrit (New Objective) analytical column packed with Waters BEH 1.7µm stationary phase using a Dionex UltiMate 3000 RSLC liquid chromatography (LC) system (Thermo Scientific). The analytical gradient for peptide separation began at 2% mobile phase B (MPB) and 98% mobile phase A (MPA) for 4min, MPB was then increased to 30% over 40min, raised to 40% MPB over 20min,

increased to 95% over 10min, held for 2min, returned to 2% B in one minute and equilibrated for 15min. MPA was composed of 98:2 (water/acetonitrile) with 0.2% FA and MPB was composed of 80:10:10 (acetonitrile/ isopropyl alcohol/water) with 0.2% FA. Analysis of the eluting peptides was performed using an Orbitrap Fusion Lumos mass spectrometer (Thermo Scientific) operated in data dependent mode. Survey scans were acquired from 300-1400m/z with 120,000 resolving power and an AGC of 4e5 and max fill time of 50ms. MS/MS scans of selected precursor ions were performed for a maximum of 3s or until the list was exhausted and dynamic exclusion was set to 45s. Quadrupole isolation for MS/MS scans was set at 0.7 m/z followed by fragmentation in the ion trap with "Rapid" scan speed and an ion target value of 5e4 and maximum injection time of 22ms using normalized collision energy of 28% from 200-1200 m/z. The monoisotopic precursor selection was set to peptide and charge states of 1, greater than 5, or unknown were excluded.

Quantitation and statistics

MS raw files were processed in MaxQuant software version 1.6.7.0 (62). Peptides were searched using the Andromeda search engine against the human Uniprot FASTA database downloaded July 24th, 2019. Cysteine carbamidomethylation was set as a fixed modification and N-terminal acetylation and methionine oxidations were set as variable modifications. Searches were performed with a false discovery rate of 1% for both peptides and proteins using a target-decoy approach. A minimum of two peptides were required, peptide length was at least 7 amino acids long and MS^2 match tolerance was set to 0.5Da.

Match between runs was enabled with a retention time window of 0.7min. Enzyme specificity was set to trypsin and a maximum of 2 missed cleavages were allowed. Protein data was extracted from the "proteinGroups.txt" file and differential quantitation was carried out in Perseus version 1.6.0.7 (63). Aerobic exercise samples were processed in three separate batches and protein quantification results were merged by gene name prior to statistical analysis. All other mass spectrometry data was processed using custom R scripts.

For all exercise data, a minimum of 60% non-zero values were required in the post exercise group and the protein intensities were $\log^2$ transformed. The data was assessed for normality and the Pre vs Post exercise data were analyzed with a paired, two sample T test with the S0 parameter set to 0.1 and a permutation based FDR threshold of $P < 0.05$ was applied to the data set.

MS raw files from the cell culture experiments and PPP vs PRP comparisonwere searched as described above. Method comparison and SEC fractionation experiment MS raw files searched against the human SwissProt FASTA database downloaded February 2017, all other parameters are as described above, Proteomics, nFLC and NTA time course analysis measurements of total EV abundance were analyzed using a one tailed two sample T test and data is displayed as mean ± SEM. Plasma concentrations obtained from the plasma proteome database for EV enriched proteins and contaminants were compared using the Mann-Whitney U test. All other comparisons were performed using a two tailed two sample T test.

Pathway and functional enrichment analysis

Functional annotation enrichment analysis was carried out using DAVID Bioinformatics Resources functional annotation tool (v6.8). Enrichment p values were FDR corrected using Benjamimi-Hochberg procedure and gene sets with a p value ≤ 0.05 were reported. Proteins that were statistically up or down regulated after exercise were subjected to Ingenuity Pathway Analysis (IPA) and regulated canonical pathways with a -log(p-value) ≥ 1.3 and a non-zero z-score were reported. For cell culture experiments, proteins identified uniquely in each cell type were subjected to an overrepresentation enrichment analyzed (ORA) using WEBGESTALT software. Redundancy of enriched gene sets was then reduced with the affinity propagation method using the R package apcluster and gene sets passing FDR (Benjamimi-Hochberg procedure ≤ 0.05) were reported.

Chapter 3: Multi-omics analysis of exercise resistance in obese individuals

Introduction

Obese individuals suffer from derangements in skeletal muscle, including mitochondrial impairments, oxidative stress, insulin resistance, and reduced myocellular quality. As skeletal muscle is the primary site of macronutrient metabolism, a process that is dysregulated in obese individuals, improving the quality of skeletal muscle is an important consideration in the treatment of obesity. At present, obesity accounts for 39% of adult Americans (64) and is defined as having body mass index (BMI) of 30 or higher. Obesity is a known risk factor for several pathologic conditions such as type 2 diabetes, cancer, cardiovascular disease and mental illness among others (65,66). If current trends continue, nearly half of US adults will be obese by 2030(67), which would drastically increase the annual obesity related healthcare costs that have already been estimated at more than 190 billion (68).

Similar to aged individuals, it appears that muscle of obese individuals is resistant to the anabolic action of resistance exercise regimes as well as protein ingestion in comparison to normal weight adults (12,69). This so called anabolic, or exercise resistance leads to impaired muscle protein synthesis which contributes to poor muscle health in obesity. The underlying cause of exercise resistance is likely related to insulin resistance, intramuscular/systemic inflammation, or lipid accumulation (70), however, the precise molecular mechanisms underpinning this phenomenon are not currently understood. To identify and characterize dysregulated cellular processes that may contribute to exercise

resistance in obesity, we performed a quantitative multi-omics comparison of the transcriptome, proteome and phosphoproteome in muscle tissue from lean and obese individuals before and after and acute bout of aerobic exercise. The aim of our study was to identify dysregulated pathways and find potential therapeutic targets that could help enhance the benefits of exercise in obese patients with exercise resistance.

Results

Quantitative multi-omics analysis of lean and obese subjects. To identify baseline differences, and differences in responsiveness to exercise between lean and obese subjects we recruited 8 individuals (obese, n = 4; lean, n = 4) to perform one bout of cycling at 70% Vo2max using only the left leg. For baseline comparisons, muscle biopsies were obtained from the right v. lateralis one day prior to the acute exercise bout. To determine how the single bout of exercise regulated exercise-responsive genes we collected post-exercise muscle biopsies 3hr following exercise. We then carried out a multiplexed quantitative proteomics and phosphoproteomics analysis in addition to transcriptome profiling of the muscle biopsy samples to investigate systems level regulation of exercise related signaling pathways in the lean and obese individuals at the two timepoints. To perform the proteome analysis, protein was extracted from muscle tissue, digested with trypsin and labeled with tandem mass tags (TMT). The labeled peptides were then fractionated and analyzed by nano-LC-MS/MS on an Orbitrap Fusion Lumos mass spectrometer (Thermo Scientific, San Jose CA). After filtering decoy sequences and common contaminants, 4981 proteins were identified and 9979 phosphosites were localized. At baseline, 64 proteins were upregulated and 51 were downregulated (adj.p-val

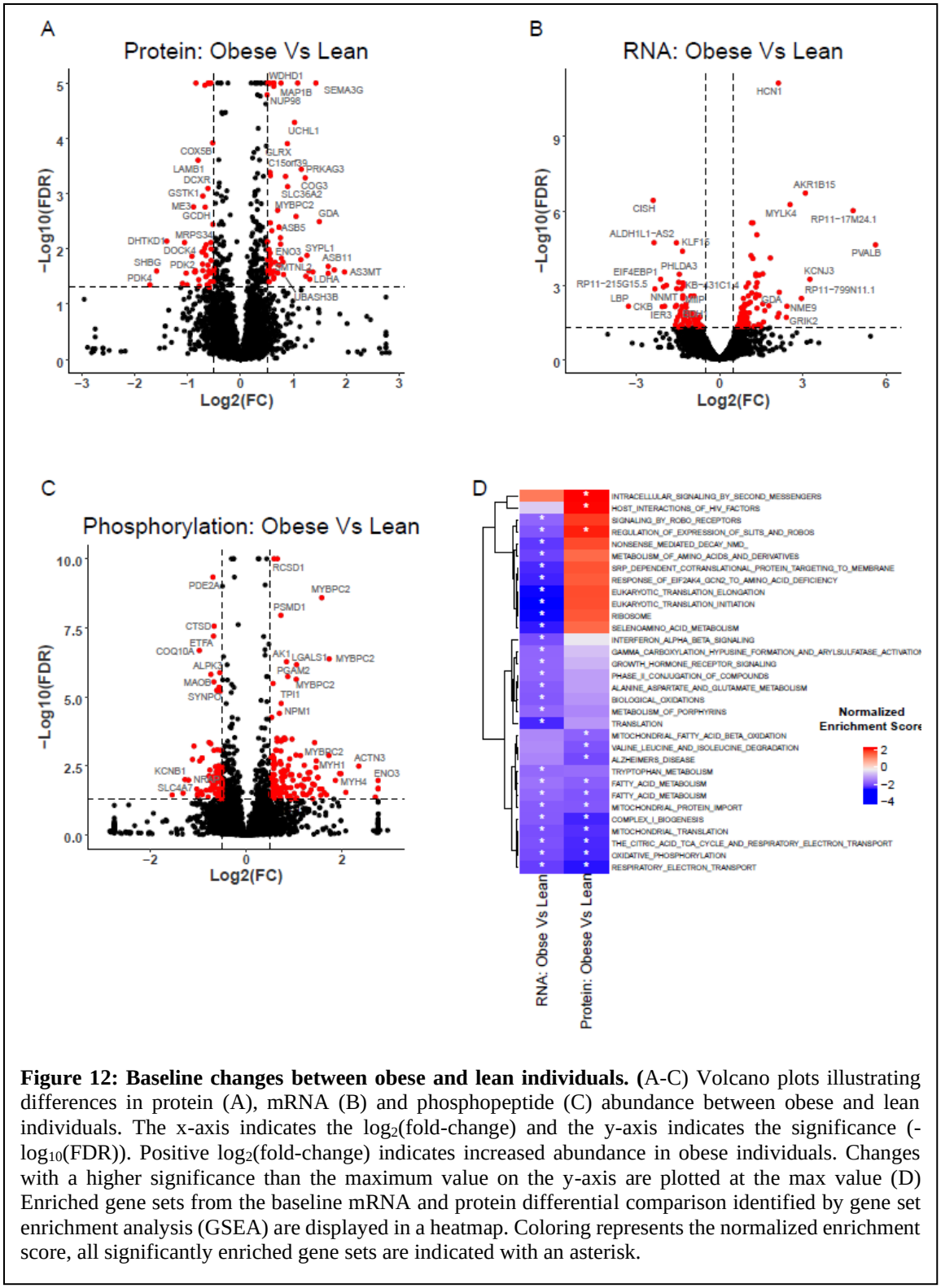

Figure 12: Baseline changes between obese and lean individuals. (A-C) Volcano plots illustrating differences in protein (A), mRNA (B) and phosphopeptide (C) abundance between obese and lean individuals. The x-axis indicates the $\log_2$(fold-change) and the y-axis indicates the significance (-$\log_{10}$(FDR)). Positive $\log_2$(fold-change) indicates increased abundance in obese individuals. Changes with a higher significance than the maximum value on the y-axis are plotted at the max value (D) Enriched gene sets from the baseline mRNA and protein differential comparison identified by gene set enrichment analysis (GSEA) are displayed in a heatmap. Coloring represents the normalized enrichment score, all significantly enriched gene sets are indicated with an asterisk.

< 0.05, log2(fold-change) > ±0.5) in obese individuals relative to lean (**Figure 12A**). At

the phosphorylation level, 139 phosphosites were

upregulated and 51 were downregulated in obese subjects relative to lean controls using the same significance thresholds (**Figure 12C**). Interestingly, the majority of phosphorylated peptides were not regulated at the protein level, suggesting that phosphorylation signaling is altered in the obese subjects (data not shown). At the mRNA level, 13175 transcripts were identified of which 97 were upregulated and 65 were downregulated in obese subjects relative to lean controls (**Figure 12B**). In total, quantitative measurements were obtained for 27679 molecules.

To investigate systems level pathway alterations in the obese subjects we identified enriched gene sets in the proteomics and transcript data using gene set enrichment analysis (GSEA) and merged the results in a heatmap (**Figure 12D**). As expected, gene sets related to mitochondrial translation and oxidative phosphorylation were negatively enriched in obese subjects at the transcriptome and proteome level. Mitochondrial impairments are well characterized in the pathogenesis of obesity (71). In addition to mitochondrial impairments, decreased muscle protein synthesis is thought to play a role in impaired muscle function and quality in obese individuals (69). In line with previous reports, signatures of reduced protein synthesis were identified in obese subjects at the transcript, but not protein level. Interestingly, several proteins involved in protein translation including EIF4G3, EIF2B5, EIF4A2 and EIF4G1were upregulated in obese subjects, raising the possibility that increased stability of these proteins could be a compensation for decreased transcript levels of ribosomal and translation initiation complex proteins in obese subjects.

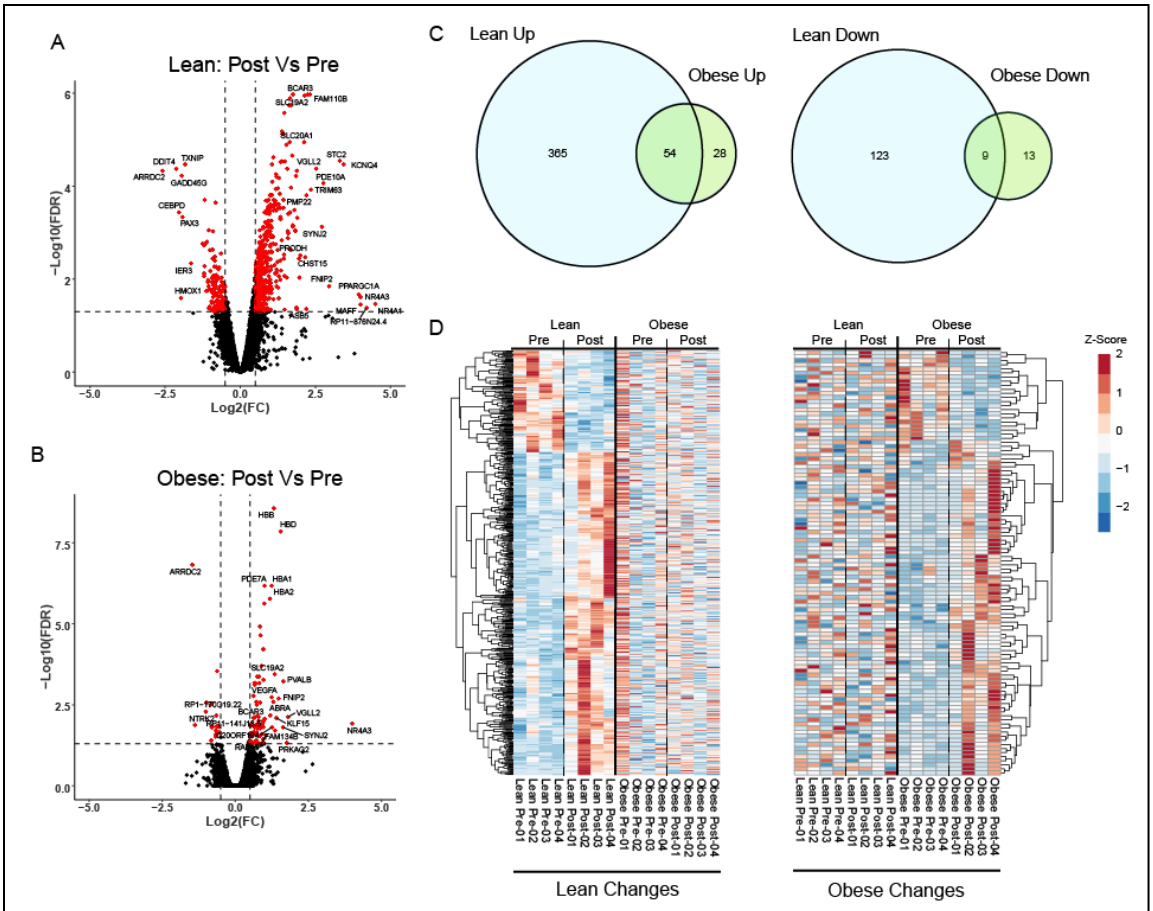

Figure 13: Transcriptome changes after exercise in obese and lean individuals. Differences in transcript abundance after exercise are displayed in volcano plots for lean (A) and obese (B) individuals. The x-axis indicates the $\log_2$(fold-change) and the y-axis indicates the significance ($-\log_{10}$(FDR)). Positive $\log_2$(fold-change) indicates an increase in transcript abundance after exercise. (C) Transcripts which are upregulated (left) and downregulated (right) after exercise are compared between obese and lean individuals with a Venn-diagram. (D) Transcripts significantly altered after exercise are clustered and displayed in a heatmap. (Left) Transcripts altered by exercise in lean individuals are displayed with the corresponding changes in obese individuals to illustrate differences in the response to exercise between the two groups. (Right) Transcripts significantly altered in obese individuals are shown with corresponding changes in lean individuals.

Next, we examined phosphosite-centric kinase activity enrichment using PTM-SEA (72). This analysis identified the significant regulation (FDR < 0.1) of several kinases. For instance, inferred kinase activities for PAK1, ERK1/MAPK3, GSK3B and PRAKA were downregulated in obese subjects while the activities of others such as

p90RSK/RPS6KA1, PLK1, AKT1, PKCA/PRKCA and CDK1 were upregulated (**Figure 15D**).

Lean and obese subjects display different responses to exercise. To characterize differences in the molecular response to exercise between the lean and obese subjects, we performed a differential analysis comparing the post-exercise timepoint to the pre-exercise timepoint for each group. The response to exercise at the transcript level was markedly different between groups. In the lean group, 419 transcripts were upregulated and 132 were downregulated after exercise with an adjusted p-value < 0.05 and log fold-change > ± 0.5 (**Figure 13 A-C**). In contrast, only 82 transcripts were increased and 22 were decreased after exercise in the obese group and minimal overlap resulted unique responses in each group (**Figure 13D)**. Unique responses to exercise in each group were also observed at the protein level where the upregulation of 68 proteins and downregulation of 18 proteins was observed in lean group (**Figure 14 A-C**). In comparison only 20 proteins were upregulated in the obese group whereas 40 were downregulated leading to distinct responses within each group (**Figure 14E**). To study systems level regulation we again performed gene-centric pathway enrichment using GSEA and merged transcript and protein results in a heatmap to visualize coordinated pathway changes (**Figure 14D**). At the transcript level, multiple gene sets were significantly regulated in the lean group. This includes the downregulation of multiple gene sets related to mitochondrial translation and oxidative phosphorylation. Additionally, several gene sets were enriched after exercise in the lean group including signaling by receptor tyrosine kinases. None of these pathways, however, were enriched at the protein level. This may reflect the acute nature of exercise training

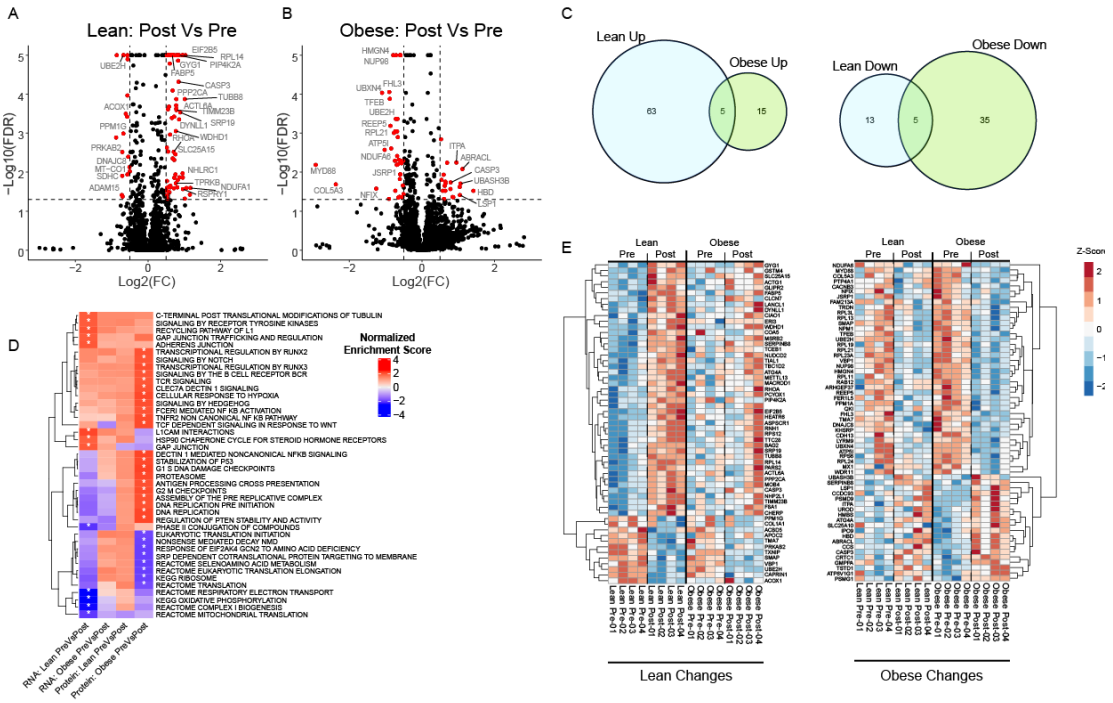

Figure 14: Proteome changes after exercise in obese and lean individuals. Exercise induced changes in protein abundance are displayed in volcano plots for lean (A) and obese (B) individuals. The x-axis indicates the $\log_2$(fold-change) and the y-axis indicates the -$\log_{10}$ value of the false discovery rate (FDR). Positive $\log_2$(fold-change) indicates an increased protein abundance after exercise. (C) Proteins which are upregulated (left) and downregulated (right) after exercise are compared between obese and lean individuals in a Venn-diagram. (D) Enriched gene sets identified in the transcript and protein exercise comparison are displayed in a heatmap to illustrate pathway regulation at a systems level. Color represents normalized enrichment score, all significant changes (adjusted p-value < 0.05) are indicated with an asterisk. (E) Proteins significantly altered after exercise are clustered and displayed in a heatmap. (Left) Proteins altered by exercise in lean individuals are displayed with the corresponding changes in obese individuals to illustrate differences in the response to exercise between the two groups. (Right) Proteins significantly altered in obese individuals are shown with corresponding changes in lean individuals.

and the timepoint at which the post exercise sample was collected and suggests that protein level changes had not occurred by 3hr post exercise. Interestingly, in contrast to the lean group no regulated gene sets were identified at the transcript level in the obese group, however, multiple gene sets were regulated at the protein level. Regulated pathways at the protein level include downregulation of multiple gene sets related protein translation including ribosome and eukaryotic translation initiation. Multiple upregulated gene sets

after exercise in the obese group were related to proteasomal degradation including proteasome antigen processing and cross presentation. Previous reports have demonstrated alteration in the ubiquitin proteasome system (UPS) in obesity and insulin resistance, but the effect of exercise on the UPS in muscle has not been studied. Insulin resistance increased degradation of muscle protein through a mechanism which involves suppression of PI3K/AKT signaling and activation of the UPS (73). Additionally, skeletal muscle cells from obese donors display elevated proteasomal activity and decreased flux through the autophagic/lysosomal pathway (74). Our findings, together with previous reports suggest that reduced protein synthesis together with increased proteasomal activity after exercise in obese subjects may contribute to poor muscle tissue maintenance and reduced muscle quality.

We next evaluated differences in regulation of phosphorylation after exercise in the lean and obese groups. Differential analysis of the pre- and post-exercise timepoints identified upregulation of 229 phosphosites after exercise while 25 were downregulated. Similar to the transcript and protein level, obese subjects displayed a markedly different response to exercise at the phosphorylation level. After exercise, only 56 phosphosites were upregulated in the obese group whereas 44 were downregulated (**Figure 15 A-C**). Minimal overlap of regulated phosphosites suggests that the lean and obese groups have unique alteration in phosphorylation after exercise (**Figure 15C**). To identify regulated signaling pathways and kinase activity after exercise in each group we again utilized PTM-SEA (**Figure 15D**). This analysis identified increased activity of 4 kinases after exercise in the lean group including Erk1/MAPK3, GSK3B and PKCD, however, none of these kinases

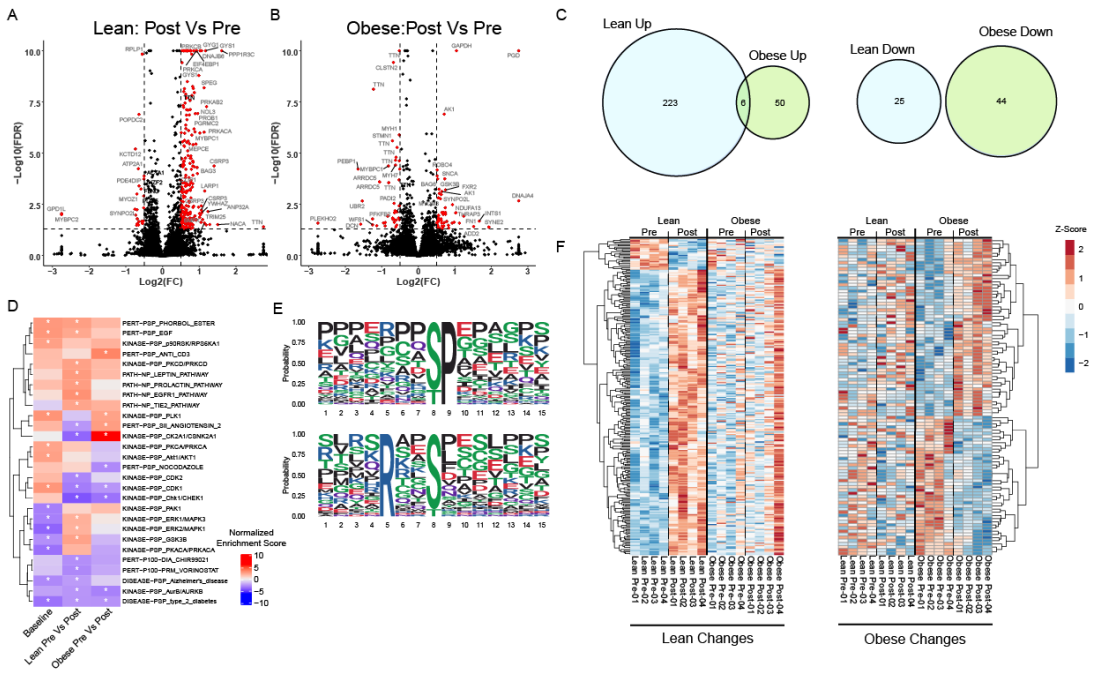

Figure 15: Phosphoproteome changes after exercise in obese and lean individuals. Exercise induced changes in phosphorylation are displayed in volcano plots for lean (A) and obese (B) individuals. The x-axis indicates the $\log_2$(fold-change) and the y-axis indicates the $-\log_{10}$ value of the false discovery rate (FDR). Positive $\log_2$(fold-change) indicates an increased protein abundance after exercise. (C) Phosphopeptides which are upregulated (left) and downregulated (right) after exercise are compared between obese and lean individuals in a Venn-diagram. (D) Enriched phosphorylation signatures obtained from PTM-signature enriched enrichment analysis (PTM-SEA) are displayed in a heatmap to illustrate regulation of signaling pathways. Enriched phosphorylation signatures identified from the baseline comparison of lean and obese individuals are displayed (left) next to enriched phosphorylation signatures after exercise in lean (center) and obese (right) individuals. Color represents normalized enrichment score, all significant changes (adjusted p-value < 0.05) are indicated with an asterisk. (E) Sequences logos for enriched phosphorylation motifs identified in exercise induced changes from lean individuals using the Motif-X algorithm are displayed. (D) Proteins significantly altered after exercise are clustered and displayed in a heatmap. (Left) Proteins altered by exercise in lean individuals are displayed with the corresponding changes in obese individuals to illustrate differences in the response to exercise between the two groups. (Right) Proteins significantly altered in obese individuals are shown with corresponding changes in lean individuals.

were significantly increased after exercise in the obese group. In the obese group, activity of PLK1 was increased after exercise. Interestingly, the activity of CK2A1 (casein kinase 2) was upregulated after exercise in the obese group and downregulated after exercise in the lean group. Interestingly, previous reports have shown that CK2 activity inhibits the

conversion of white adipocytes into beige adipocytes (75). White adipocytes are simply fat

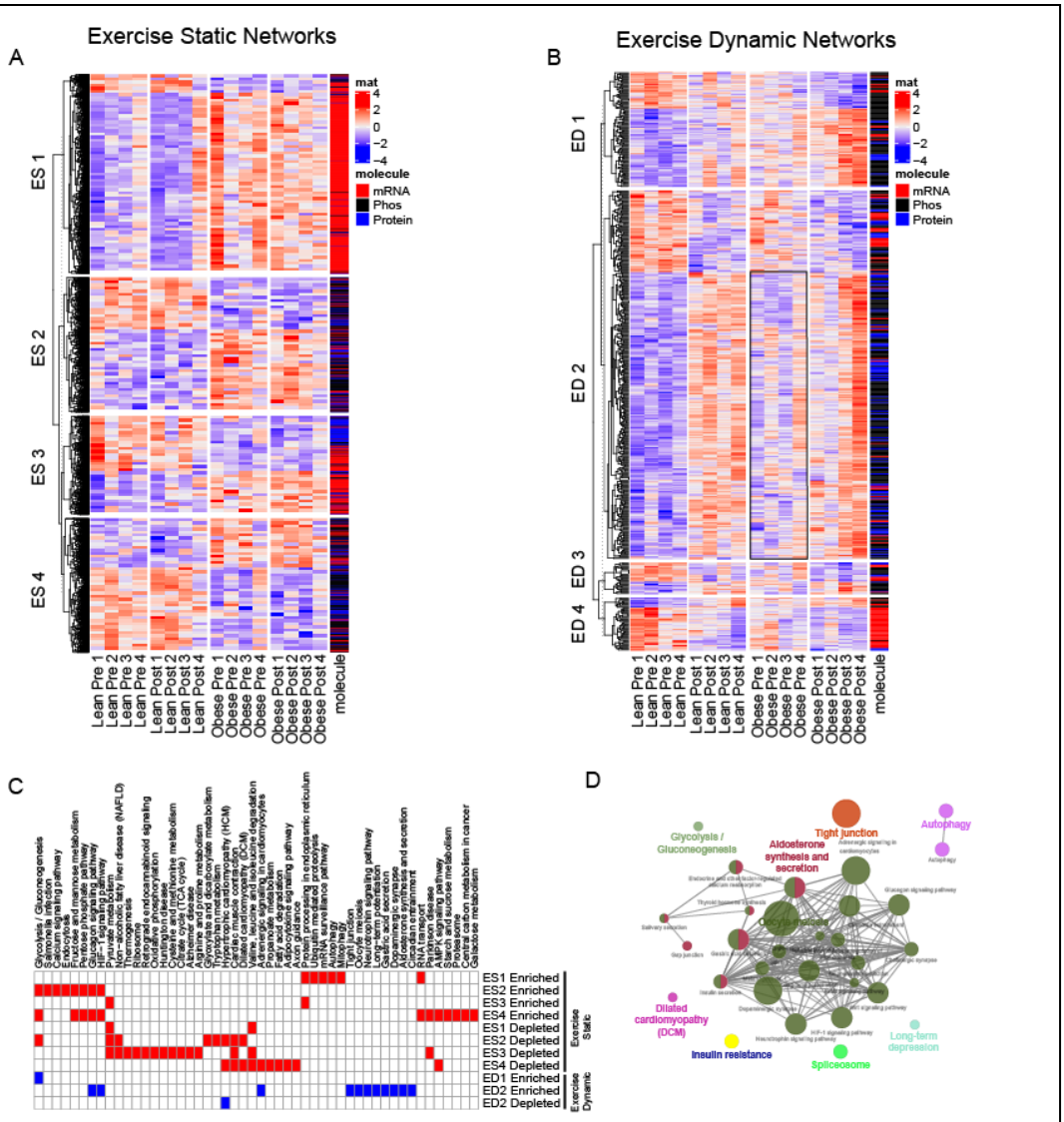

Figure 16: Integrated multi-omics network analysis identifies altered network modules in obese individuals. Transcriptome, proteome and phosphoproteome data was z-transformed and merged into a single matrix for weighted correlation network analysis (WCGNA) to identify modules of co-regulated molecules that associate with phenotypic traits. (A,B) The two most significant positively and negatively correlated network modules associated with obesity status ("Exercise Static", A) and obesity status and exercise ("Exercise Dynamic", B) are plotted in a heat map and separated by module (rows) and sample group (columns). Molecule type (i.e. mRNA, protein or phosphopeptide) is color-coded as indicated by the bar on the right. (C) Summary of enriched pathways in exercise static or exercise dynamic network modules. A two-sided hypergeometric test was performed to obtain p-values, and correction was carried out with Bonferroni step down. A significance threshold of adjusted p-value = 0.05 was applied and significant pathways are indicated by color. Significant exercise static pathways are colored red, significant exercise dynamic pathways are blue. (D) Figure representing enriched pathways from the exercise dynamic network module 2.

storage depots, whereas brown adipocytes are metabolically active and produce heat via

mitochondrial uncoupling. Beige adipocytes are thought to be white adipocytes that respond to stimuli and share properties more similar to brown adipocytes (75). The observation that CK2A1 is downregulated after exercise in lean, but upregulated in obese suggests dysregulated brown adipocyte formation in obese individuals may be related to altered CK2 signaling in muscle tissue after physical activity. Although these findings are promising, further experiments are required to fully characterize the biological significance of CK2 signaling in muscle after exercise.

Integrative Multi-omics analysis identifies clusters of molecules associated with the obese phenotype and differential responses to exercise. Next, we leveraged the multi-omics data to identify clusters of molecules associated with obesity status and exercise timepoints. Towards this goal the proteome, phosphoproteome and transcriptome data were transformed to the same scale and merged prior to weighted gene co-expression network analysis (WCGNA) (76,77). WCGNA identified 100 functional modules. The four modules most significantly correlated with obesity status (**Figure 16A**) and exercise time point (**Figure 16B**) were then subjected to functional enrichment analysis in ClueGo (**Figure 16C**). As modules associated with obesity status did not change with exercise, they were termed "exercise static" (ES), whereas modules associated with exercise timepoint were termed "exercise dynamic" (ED). Each exercise refractory and exercise dynamic module had varying molecular composition. For instance, exercise refractory module 1 was composed primarily of mRNA and was significantly enriched (adj.p-value < 0.05) for molecules involved in pathways such as ubiquitin mediated proteolysis, autophagy, and protein processing in the ER, all of which were increased in obese individuals relative to

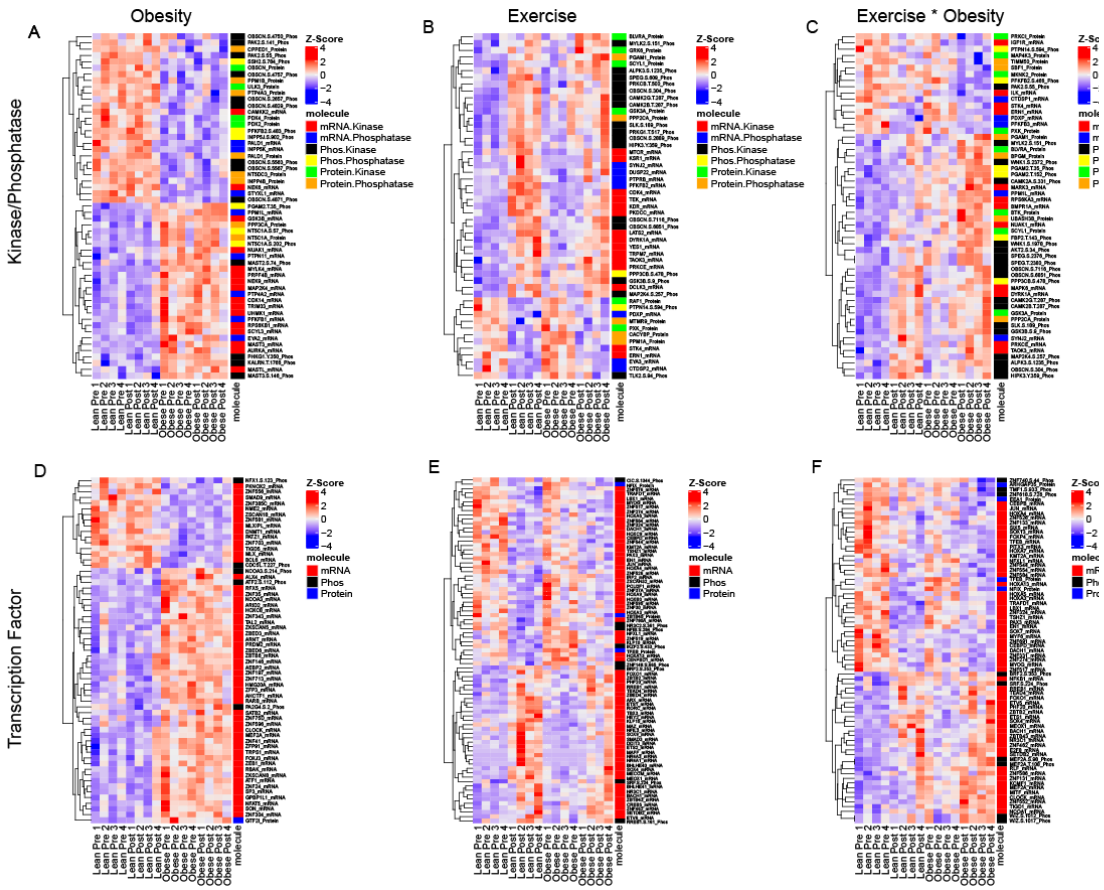

Figure 17: Network analysis of kinases, phosphatases and transcription factors reveals dysregulation of signaling networks in obese individuals. Kinase and phosphatase transcripts, proteins and phosphopeptides with significant network module phenotype associations were clustered to identify alterations in signaling molecules that associate with obesity and the response to exercise. Kinase and phosphatase transcripts, proteins and phosphopeptides that associate with obesity status (A), exercise status (B) or obesity status and exercise are displayed in a heatmap. Molecules in each heatmap were filtered by module p-value in order to display row labels. The color or each row represents z-score. The molecule class is color coded as indicated by the car on the right. Transcription factor transcripts, proteins and phosphopeptides that are significantly associated with obesity status (C), exercise status (D), or obesity and exercise (E) are displayed in a heatmap. Molecule class is as indicated by the color coded bar on the right of each heatmap.

lean. Exercise refractory module 2 was driven by a high percentage of phospho peptides that associated with pathways such as glycolysis/gluconeogenesis, HIF-1 signaling, and glucagon signaling, which were also increased in obese individuals. Exercise responsive molecules also displayed varying molecular composition. Exercise responsive module 2

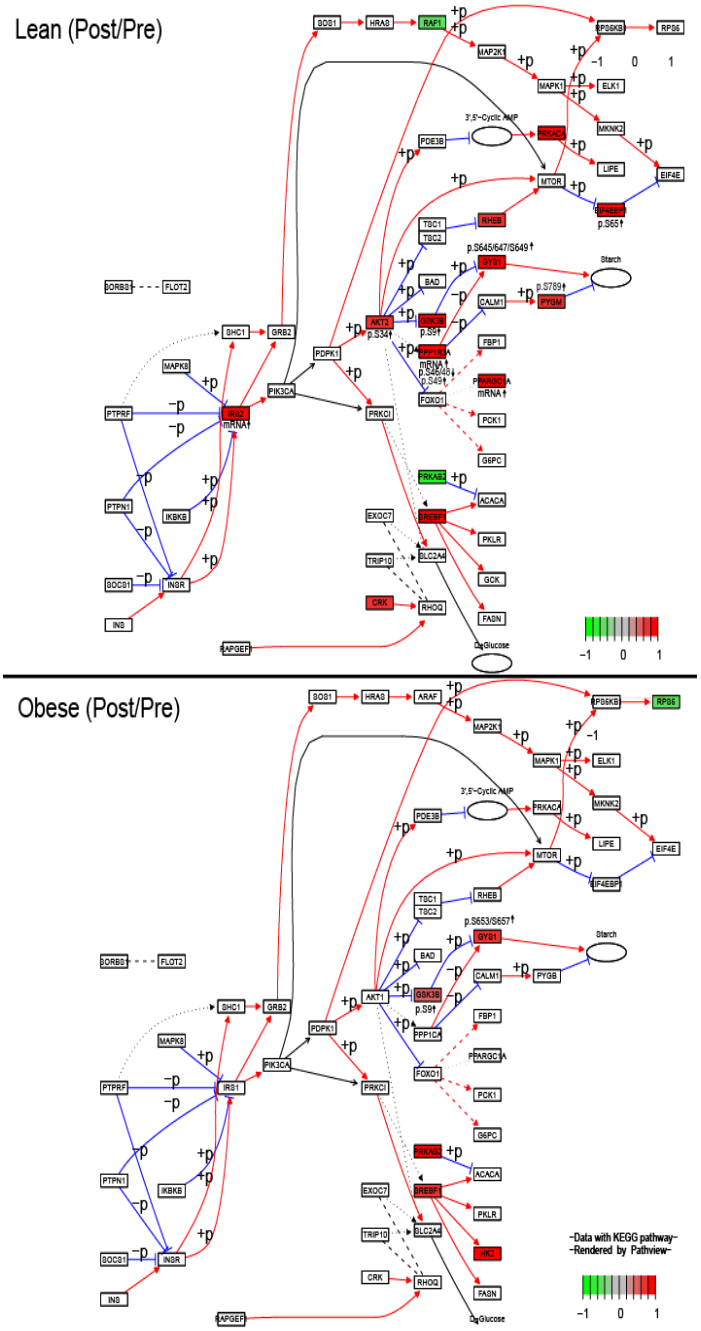

Figure 18. Pathway based quantitative data integration of exercise induced changes in lean and obese subjects. Differential expression analysis of transcript, phosphorylation and protein level data are overlaid on the Kegg insulin signaling pathway. Molecules with significant changes after exercise (adjusted p-value < 0.05 and $\log_2$ fold change > 0.5) are colored according to their $\log_2$ fold change. Post/Pre exercise changes for lean individuals are indicated on the top graph, whereas Post/Pre exercise changes for obese individuals are indicated on the bottom graph. Functionally characterized phosphosites are indicated by black text and phosphosites that are currently uncharacterized are indicated by grey text. Molecular interactions are indicated by red(positive regulation) and blue (negative regulation) lines.

was composed of primarily protein and phosphopeptides which were significantly enriched for molecules involved in processes such as long term potentiation, tight junctions and neurotrophin signaling (**Figure 16B,D**).

Lean and obese subjects displayed large differences in phosphorylation after acute exercise. Therefore, to further investigate the underlying cause of the differential phosphorylation signaling that occurred in lean and obese subjects after exercise we clustered all transcripts, proteins and phosphopeptides derived from kinases and phosphatases that belonged to modules significantly associated with obesity and exercise status by WCGNA. This analysis identified clusters of kinases and phosphates associated with obesity status (**Figure 17A**) exercise timepoint (**Figure 17B**) and both exercise and obesity (**Figure 17C**). Further, we performed the same analysis for transcription factors (**Figure 17 D-F**). Transcription factors also formed clusters associated with obesity status, exercise timepoint and both. Transcription factors are generally present at very low levels, therefore, it is not surprising that the clusters were composed primarily of transcripts.

Dysregulated glycogen synthesis signaling is associated with obesity. Integration of multi-omic kinase and phosphatase data using WCGNA uncovered a dysregulation of GSK3β signaling in obese subjects. GSK3β mRNA was associated with obesity status, where higher levels were observed in obese subjects (**Figure 17A**). Further investigation found that obese subjects also displayed increased phosphorylation of GSK3β at S9, a known inactivating phosphorylation event (78). After exercise, phosphorylation of S9 increased in both groups, however, GSK3β and GSK3α protein levels increased only in the lean group (**Figure 17B, 18**). GSK3β is a serine/threonine kinase and important regulator of cellular metabolism in addition to proliferation, migration, cell death and

immune function (79-81). GSK3β phosphorylates and inactivates GYS (82), leading to reduced glycogen synthesis. Additionally, after exercise lean individuals displayed upregulated PPPR3A mRNA and decreased phosphorylation on S46, a known activating phosphorylation whereas obese individuals displayed no change (**Figure 18**). PPPR3A, also known as GM, is a regulatory subunit of protein phosphatase-1 (PP-1) expressed in muscle which recruits and positively regulates GYS by dephosphorylation (83). These data indicate that exercise induces mRNA, protein and phosphorylation level changes after exercise in lean individuals that modulate glycogen synthesis, whereas obese individuals do not display the same alterations. Previously, mice expressing phosphorylation resistant GSK3β were shown to be resistant to metabolic disorder characterized by insulin resistance, obesity and dyslipidemia through a process which involved GSK3β-dependent upregulation of the hormone adiponectin (84). Interestingly, obese subjects in the present study also displayed decreased levels of adiponectin relative to lean subjects at baseline. Taken together, these data indicate that GSK3β signaling is dysregulated in obese subjects which may alter glycogen synthesis and result in reduced muscle quality in obese individuals. GSK3β has been evaluated as a therapeutic target in other pathological conditions such as cancer (85). Therefore, GSK3β is a potential a point of therapeutic intervention in obesity induced muscle derangements and warrants further investigation. Although several molecules involved in GSK3β signaling are dysregulated in obese subjects in the present study, others have shown that glycogen synthesis is not altered in subjects with type II diabetes and obesity after exercise relative to lean individuals (86). This study, however, utilized western blots to evaluate GYS phosphorylation levels.

Western blots are known to un-specific and should be confirmed by more specific methodologies such as mass spectrometry. Never the less, these results are discrepant and further studies are required to characterize alteration in GSK3β signaling in obese subjects after exercise.

Discussion:

Obesity is a known risk factor for several chronic conditions, and muscle of obese individuals has been shown to have impaired mitochondrial function, reduced protein synthesis rates and reduced myocellular quality. In this study, we used a multi-omics approach to elucidate molecular aberrations that underlie poor muscle tissue health in obese individuals. At baseline, we found signatures of reduced oxidative phosphorylation and mitochondrial protein translation using gene centric GSEA (**Figure 12, D**). In addition, GSEA identified reduced levels of protein synthesis in obese individuals, another hallmark of exercise resistance in obesity. The identification of known impairments in obese muscle in this data set indicate the quality of this data set, and provide confidence that novel alterations uncovered in this study are accurate even though a limited number of subjects per group were available.

Relative to lean subjects, obese subjects displayed markedly different responses to exercise at the transcript level (**Figures 13, A-D**) protein level (**Figure 14, A-C,E**) and phosphorylation level (**Figure 15, A-C, F**). In lean individuals, integrated gene centric pathway analysis identified a decrease in mitochondrial translation and oxidative phosphorylation at the transcript, but not protein level after exercise. Lean individuals also displayed an increase in receptor tyrosine kinase signaling after exercise whereas obese

individuals did not. Interestingly, dysregulated receptor tyrosine kinase signaling has been implicated in obesity and is the current focus of several research groups (87,88). In obese individuals, GSEA identified decreased levels of protein translation together with increased proteasomal activity. These findings, suggest that reduced protein synthesis together with increased proteasomal activity after exercise in obese subjects may contribute to poor muscle tissue maintenance and reduced muscle quality.

At the phosphorylation level, PTMSEA identified the enrichment of several kinase signatures including Erk1/MAPK3, GSK3B and PKCD. Importantly, none of these kinases were significantly increased after exercise in the obese group. Additionally, the activity of CK2 was decreased after exercise in the lean group whereas its activity was increased after exercise in the obese group. In adipose tissue, CK2 has previously been shown to inhibit the conversion of white adipocytes to more metabolically active beige adipocytes (75). Beige adipocytes are thought to be white adipocytes that respond to stimuli and share properties more similar to brown adipocytes (75). Thus, the observation that CK2 is downregulated after exercise in lean, but upregulated in obese suggests dysregulated brown adipocyte formation in obese individuals may be related to altered CK2 signaling in muscle tissue after physical activity. Although the significance of CK2 signaling after exercise in lean and obese individuals requires further investigation, this observation suggests that dysregulated CK2 signaling may underlie metabolic alterations in obese individuals and future studies are warranted.

Multi-omics integration identified networks of regulated kinases, phosphatases and transcription factors associated with obesity status and exercise timepoint. Additionally,

integration of transcript, proteome, and phosphorylation data by WCGNA identified dysregulated GSK3β signaling in obese individuals at baseline, and after exercise. Baseline comparison of phosphorylation profiles between lean and obese subjects uncovered increased phosphorylation of GSK3β as serine-9. After exercise, phosphorylation of GSK3β at serine-9 increased in lean and obese individuals, however, 3 phosphosites on GYS (serine 641, 645, 649) were reduced in lean individuals but not obese. Phosphorylation of GYS inactivates glycogen synthesis, while de-phosphorylation increases activity. These data indicate that GYS is inactivated after exercise in obese, but not lean. Further two phosphosites on PP-1, the phosphatase that positively regulates GYS were increased after exercise in lean, but not obese. Collectively, these alterations indicate that GSK3β signaling, and likely glycogen synthesis are dysregulated in obese, relative to lean individuals. Previous studies have suggested that glycogen synthesis is not altered in obesity (86), however this study utilized western blots to quantify differences in phosphorylation of GYS. The fact that multiple levels of GSK3β signaling are regulated in this study and considering that we utilized mass spectrometry, a technique with much higher specificity relative to western blot, these data warrants further investigation of GSK3β signaling in obesity.

Conclusion:

In this study, we utilized a multi-omics approach to identify systems level alterations in obese individuals at baseline and in response to exercise relative to lean subjects. After exercise, obese individuals displayed deficits in protein synthesis along with

increases in pathways related to proteasomal degradation, which we hypothesize may cause unbalanced myocellular homeostatis and exercise resistance. Obese individuals also displayed significant differences in phosphorylation profiles after exercise, and reduced kinase activity. Of interest is a reciprocal regulation of CK2 in lean and obese subjects after exercise, which may play a role in adipose tissue browning. Finally, we identified dysregulated GSK3β signaling in obese individuals after exercise and suggest that future studies should investigate these alterations in the context of exercise resistance.

Methods:

RNAseq. RNA was extracted from powdered muscle biopsy samples using the Qiagen RNeasy mRNA extraction kit and sent to the Mayo Clinic Genome Analysis Core for sequencing. Briefly, libraries were prepared using the Illumina Stranded mRNA Prep and sequenced on an Ilumina HiSeq 4000. Reads will be aligned using STAR RNA-seq aligner. Differential expression analysis was carried out using a negative binomial generalized log-linear model in the edgeR R package.

Protein extraction and digestion

Muscle samples were powdered and protein was extracted with 8M urea in 100mM TEAB containing HALT™ phosphatase inhibitor cocktail (Thermo Scientific, Waltham, MA). Samples were then probe sonicated to ensure complete homogenization, and protein content was estimated by BCA assay (Pierce, Waltham, MA). Disulfide bonds were

reduced and alkylated with10mM TCEP and 10mM IAA at RT for 30min while protected from light. Trypsin/LysC Mix (Promega, Madison, WI) was added at a 1:50 enzyme to protein ratio and samples were digested overnight (16hr) at 37°C. The enzymatic digest was terminated by adding TFA to a final concentration of 0.2% and peptides were desalted using a 10mg Strata-x PSVDB cartridge (Phenomenex, Torrance, CA), dried, and reconstituted in 100µl of 50mM TEAB. Peptide concentration was determined using a Pierce Colorimetric peptide assay and 95µg from each sample was labeled with TMT-Pro (Thermo Scientific) for 1hr.

High pH reversed phase fractionation

TMT labeled peptides were fractionated by high pH reversed phase liquid chromatography on Dionex Ultimate 3000 (Thermo Scientific, Waltham, MA). Peptides (1.6 mg) were separated on a 4.6 mm x 50 cm x 3.5µm Xbridge column (Waters, Milford, MA) with a 2 h gradient from 2 to 40% B mobile phase B (MPB). MPA was composed of 20 mM ammonium formate in water and MPB was composed of 20 mM ammonium formate in 80% ACN. A total of 96 fractions were collected and concatenated into 48 fractions. A 20 µg equivalent of each fraction was set aside for global proteome analysis and the rest of each sample was concentrated into 24 fractions and dried prior to phosphopeptide enrichment.

Phosphopeptide enrichment

Each fraction was reconstituted in 100 µl of 80% ACN in 0.1% TFA and transferred to 96 well plate. IMAC-based phosphopeptide enrichment was performed using Fe(III)-

NTA resin (G5496-60082) on an AssayMap Bravo (Agilent Technologies, Santa Clara, CA) platform following the manufacture instruction.

LC-MS/MS analysis

Fractionated, TMT labeled peptides (5µg) were loaded onto a 20 mm x 0.075 mm PepMap C18 trap column with loading solvent composed of 0.1% TFA flowing at 20 µl/min using an Ultimate 3000 nano HPLC (Thermo Scientific, Waltham, MA). After 4 minutes, the 10-port valve was switched and peptides were eluted off the trap column onto a 50 cm x 75 µm ID PepMap EASY-Spray™ analytical column and peptides were separated with a 2 hr gradient from 3 to 40% mobile phase B (MPB). At 2 hr, MPB was increased to 80% over 10 min, held for 15 min, and then returned to 3% for 5 minutes to re-equilibrate the column. The flowrate was set to 300 nl/min. Eluting peptides were analyzed on an Orbitrap Fusion Lumos (Thermo Scientific, Waltham, MA) mass spectrometer operated in data dependent mode. MS1 scans were acquired from 370-1700 m/z with an orbitrap resolution of 60,000 (at 200 m/z) at least every three seconds or when no more peptides were scheduled for fragmentation. The automatic gain control (AGC) was set at 1e6 and maximum ion fill time was set to 50 ms. The most abundant peptides with a charge state between 2 and 7 were selected for fragmentation with high-energy collision induced dissociation (HCD) using a normalized collision energy of 35% and a quadrupole isolation width of 0.7 m/z. The orbitrap resolution was set to 30,000, the maximum injection time was set to 54 ms, and the AGC target was set to 2e5 whereas the dynamic exclusion was set to 30 sec using a 10 ppm mass window. For phosphopeptide

analysis, the resolution for MS/MS was set to 50,000 and the maximum injection time was set to 86 ms.

Data Analysis

MS raw files were processed in MaxQuant software version 1.6.12 (62). Peptides were searched using the Andromeda search engine against the human Uniprot FASTA database downloaded July 24th, 2019. Cysteine carbamidomethylation was set as a fixed modification and N-terminal acetylation, methionine oxidation and phosphorylated serine, threonine and tyrosine were set as variable modifications. Searches were performed with a false discovery rate of 1% for both peptides and proteins using a target-decoy approach. Peptide length was to at least 7 amino acids long and MS2 match tolerance was set to 0.02Da. Enzyme specificity was set to trypsin and a maximum of 2 missed cleavages were allowed. Protein data was extracted from the "proteinGroups.txt" file and differential quantitation was carried using a generalized linear model as previously described (56).

Gene Set Enrichment Analysis

Gene set enrichment analysis was performed using Broads GSEA software. All gene sets that were negatively enriched with an FDR corrected p-value (using the Benjamini-Hochberg procedure) < 0.05 were reported. Phosphorylation site specific signature analysis was performed using PTM signature enrichment analysis (PTM-SEA) (89) with PTMSigDB version 1.9.0. All perturbation signatures, signature sets of molecular signaling pathways, kinase substrate signatures and disease-associated signature sets with an FDR corrected p-value < 0.1 were reported.

WCGNA

The transcript, proteome and phosphoproteome data were z-transformed, merged and analyzed by WCGNA (77). Briefly, a Pearson correlation matrix was calculated and both positive and negative correlations were accepted. Eigen genes were calculated as a consensus trend for each module and additional molecules were assigned based on Pearson correlation values. The four modules most significantly correlated with obesity status and exercise timepoint were subjected to gene level pathway analysis in CludGO (90). Pathway analysis in ClueGo was performed using a two-sided hypergeometric test using information obtained from Kegg. All pathways with a Bonferroni step down adjusted p-value < 0.05 were accepted. To identify networks of regulated molecules that affect phosphorylation signaling all kinases and phosphatases assigned to network modules with a significant association to obesity status or exercise timepoint were selected and subjected to hierarchical clustering. Networks of regulated transcription factors were identified using the same approach.

Chapter 4: Extracellular Vesicles as Markers of Disease Biology in Multiple Myeloma

Introduction:

Multiple myeloma (MM) is a devastating clonal plasma cell proliferative disorder responsible for over 13,000 deaths per year in the US. MM is always preceded by a pre-malignant condition termed monoclonal gammopathy of undetermined significance (MGUS) or a more advanced pre-malignant stage termed smoldering multiple myeloma (SMM). Patients with both MGUS and SMM require continuous clinical monitoring to assess for the development of malignant plasma cells (PCs) which result in the progression to MM. At present, no single clinical or laboratory feature can distinguish between the presence of premalignant (MGUS or SMM) or malignant clonal plasma cells (MM). As a result, MGUS and SMM patients who have already started to develop malignant clonal PCs progress to MM in between their scheduled clinical monitoring visits with organ damage such as lytic bone disease and/or renal insufficiency that adversely affects their survival. Thus, novel biomarkers which reflect the presence of malignant clonal plasma cells are needed to identify patients with pre-malignant disorders such as MGUS and SMM destined to rapidly progress to MM.

At a molecular level, premalignant and malignant plasma cells are undistinguishable (91). Furthermore, the genetic and epigenetic aberrations which are necessary for the transformation of normal to malignant plasma cells are largely present in premalignant plasma cell dyscrasias (21). These observations led to an intense interest in

the bone marrow micro environment (BMM) and its role in disease progression (20,21) in the setting of MM. It is now well established that alterations in the BMM facilitate tumor growth, angiogenesis bone disease and immune evasion (20-22) which promote disease progression. The exchange of soluble factors including cytokines, growth factors and extracellular vesicles (EVs) facilitate intercellular communication between myeloma and non-myeloma cells and are now recognized as a major determinant in disease response and progression (22,92).

Results and Discussion:

Although advances in our understanding of MM disease biology are promising, there is still a need for improved tests which can monitor disease progression and predict which patients will rapidly progress to malignant disease. Extracellular vesicles (EVs), including exosomes (SEVs) and microvesicles (LEVs) have received attention for facilitating intercellular communication and may be involved in supporting disease progression by mediating cross talk between tumor cells and the surrounding microenvironment. It has also been suggested that plasma derived EVs may serve as a reservoir of potential biomarkers that can shed light on disease biology in MM has. Until recently, however, technical factors including abundant plasma protein contamination and low EV recovery have precluded useful mass spectrometry-based profiling studies of plasma derived EVs (30). Here, we used a size exclusion chromatography based EV isolation method coupled to a label-free proteomics workflow to compare protein composition and abundance of SEVs and LEVs isolated from individuals with MGUS and

MM. The results of this comparison indicate that EVs may indeed be a useful reservoir of biomarkers in the setting of MM.

Using the SEC based method, we isolated SEVs and LEVs from the plasma of MGUS (n=10) and MM (n=11) patients. In total, 2055 proteins were identified in SEVs while 2794 proteins were identified in LEVs (**Figure 1A**). While many proteins were identified commonly between the two populations of EVs, some were unique to each subtype (LEVs = 1171, SEVs = 432), indicating that these are two distinct populations of

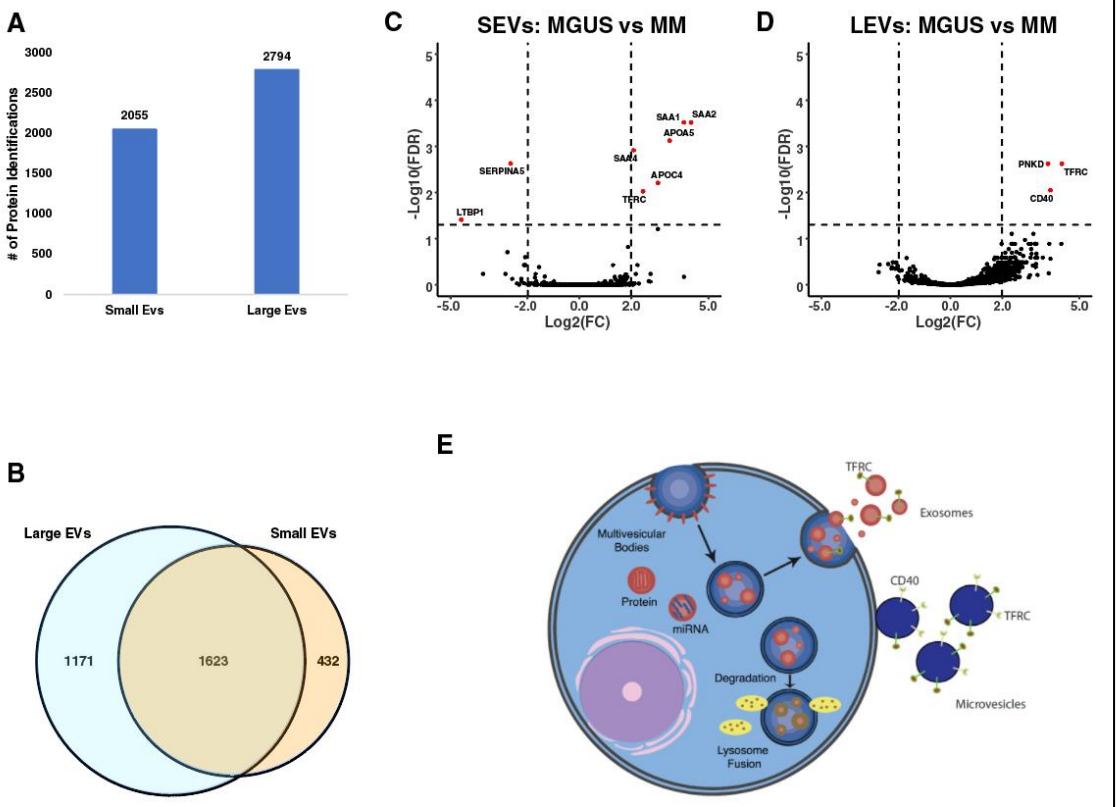

Figure 19. **Differential comparison of protein composition and abundance between subjects with MM and MGUS in SEVs and LEVs**. (A) Bar chart displaying the total number of proteins identified in SEVs and LEVs. (B) Venn diagram displaying the distribution of identified proteins in LEVs and SEVs. (C) Volcano plot illustrating differentially expressed proteins in MM relative to MGUS in SEVs and LEVs (D). positive fold change indicates increased abundance in MM. (E) Cartoon illustrating the release of CD71 (TFRC) in SEVs and LEVS and CD40 in LEVs.

vesicles. Within the SEVs, a differential comparison of protein abundance between MGUS and MM patients identified 6 upregulated and 2 downregulated proteins in MM relative to the MGUS group. Similarly, a differential comparison within the LEVs identified three upregulated proteins in the MM group relative to the MGUS group.

Interestingly, transferrin receptor (CD71) was upregulated in MM patients in both populations of EVs. CD71 is a cell surface receptor which facilities cellular iron uptake through receptor mediated endocytosis (93). In general, CD71 has a low level of expression on normal cells, however it's expression is dramatically increased in a wide variety of cancers (93,94). Anemia is also a common complication in patients with MM. A study utilizing the VK*MYC murine model of MM found high levels of CD71 expression on PCs and iron accumulation in BM macrophages, suggesting that a local depravation of iron in the BMM may lead to anemia (95). These lines of evidence suggest that PC CD71 may be shed in EVs (**Figure 1E**) and increased levels could potentially be associated with increased disease burden. However, future studies which systematically investigate this link are required.

Three isoforms of serum amyloid A, SAA1, SAA2 and SAA4 were also highly upregulated in SEVs within MM patients relative to MGUS patients (**Figure 1 C**). SAA acute phase proteins are primarily expressed in the liver and are regulated by pro-inflammatory cytokines, however, its expression has also been observed in several primary and metastatic cancer cell lines (96). SAA itself is involved in the inflammatory process

and has clinical utility as a marker of inflammation (97). Recent work has shown that SEV derived SAA levels are increased in pediatric subjects with anaplastic lymphoma kinase (ALK)-positive anaplastic large-cell lymphoma (ALCL) relative to healthy controls (98). Therefore, increased SAA levels in SEVs are associated with malignant disease and represent a potential biomarker of multiple hematological malignancies.

Next, we investigated associations between cytogenetic abnormalities and EV protein abundance by performing a differential comparison between MM patients with standard and high cytogenetic risk. This comparison uncovered a clear trend of decreased EV protein abundance in patients with high cytogenetic risk relative to those with standard risk. Within the SEVs, a total of 73 proteins were downregulated in high cytogenetic risk relative to standard risk (**Figure 2A**). Similarly, 13 proteins were downregulated in high risk relative to standard risk within the LEVS, while only three proteins were upregulated (**Figure 2B**). Cytogenetic risk groups also separate into distinct clusters (**Figure 2C,D**) despite displaying moderate inter-subject variability (**Figure 2E,F**) Interestingly, gene ontology over-representation analysis of the proteins downregulated in SEVs identified several enriched biological processes including positive regulation of immune response to tumor cells, leukocyte degranulation, chemotaxis and regulation of immune system process (**Figure 2G**) suggesting that a more functional immune response may be associated with decreased cytogenetic risk. Previous studies have shown that subjects with high risk SMM have impaired adaptive immune response relative to healthy controls (99), however,

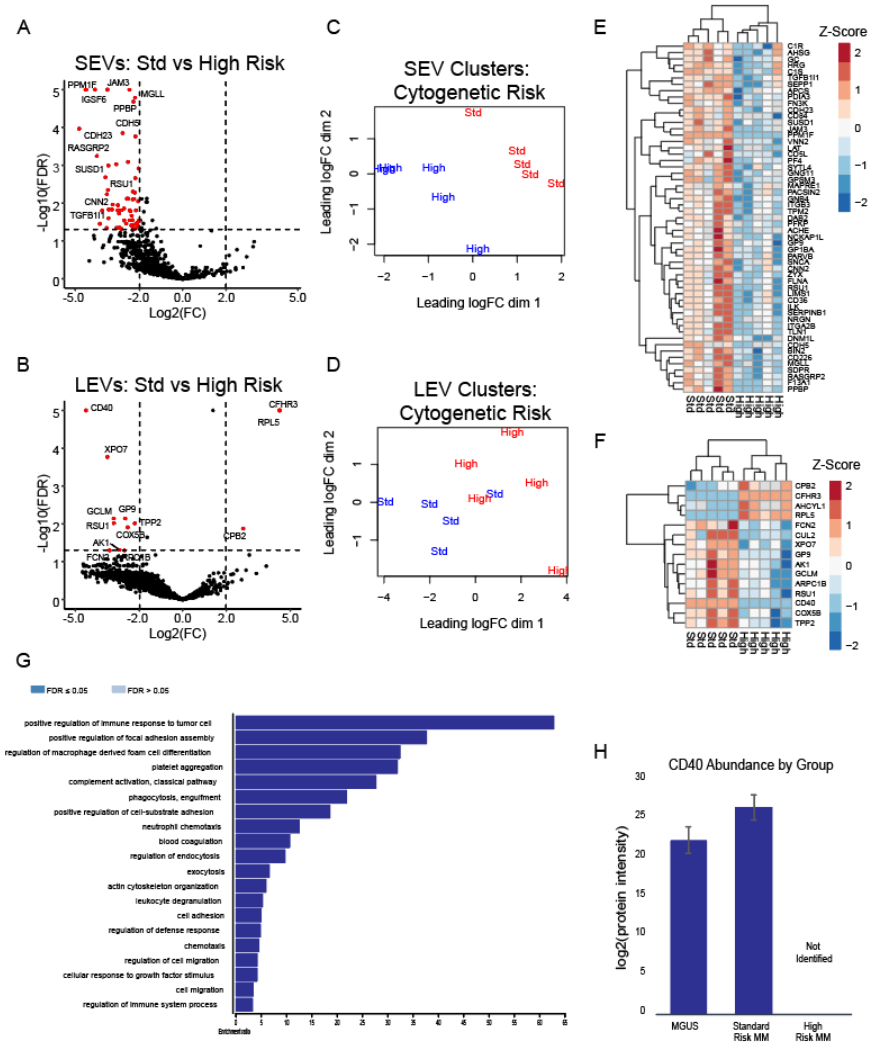

Figure 20. **Differential comparison of protein composition and abundance in abundance between subjects with high and standard cytogenetic risk**. Volcano plot illustrating differentially expressed proteins in high cytogenetic risk subjects relative to subjects with standard cytogenetic risk in SEVs (A) and LEVs (B). Multidimensional scaling (MDS) plot illustrating the distance between subjects with high and standard cytogenetic risk in SEVs (C) and LEVs (D). Heatmap illustrating inter-subject variability within differentially expressed proteins in SEVs (E) and LEVs (F). Bar plot illustrating significantly overrepresented biological processes in proteins down regulated within SEVs in subjects with high cytogenetic risk relative to standard risk. (H) Bar plot illustrating the average protein intensity of CD40 for each indicated group. Protein intensity is represented as log2(intensity).

adaptive immune response function has not been studied between high and standard cytogenetic risk.

Within the LEVs, CD40 was exclusively identified in subjects with standard cytogenetic risk. Interestingly, CD40 was also upregulated in MM relative to MGUS patients. Taken together, these data indicate that CD40 expression is increased in subjects with standard cytogenetic risk

MM relative to MGUS, however, its expression is below detectable limits or lost in subjects with high cytogenetic risk (**Figure 2H**). CD40 is a co-stimulatory receptor expressed on the surface of B cells and professional antigen-presenting cells which is required for their activation. CD40 engagement by its ligand CD40L on activated T cells regulates a diverse set of cellular processes including cellular and humoral adaptive immunity (100). The observation that CD40 was not detected in high risk subjects provides further evidence that adaptive immunity may be compromised in high risk subjects.

Conclusion:

The results of this study demonstrate that plasma EVs have the potential to serve as biomarkers of disease biology in MM. We have shown that CD71 present on SEVs and LEVs is upregulated in patients with MM relative to MGUS. This finding may have diagnostic importance and future studies which focus on the origin of this signal may shed light on mechanisms involved in progression from pre-malignant to malignant disease. We have also demonstrated that a diverse set of proteins are downregulated in EVs derived from high cytogenetic risk MM patients relative to MM patients with standard risk. In SEVs, the downregulated proteins are involved in immune function, suggesting that

immune dysregulation may be associated with high cytogenetic risk. Finally, we have shown that LEV derived CD40 is upregulated in subjects with MM relative to MGUS, but only in those with standard cytogenetic risk. CD40 was not detected in MM patients with high cytogenetic risk, suggesting that impaired adaptive immune function is correlated with high cytogenetic risk. We suggest that EVs may provide diagnostic value in MM and future studies validating these findings are warranted.

Methods

Blood collection and plasma preparation

Whole blood was drawn into ETDA tubes and placed on the benchtop for 15minutes. After 15minutes each tube was centrifuged at 2,000xg for 10min at room temperature (RT) to pellet red blood cells. The upper plasma fraction was then collected, transferred to a new sterile tube, and centrifuged again at RT for 10min at 2000xg. Platelet poor plasma was isolated by carefully transferring the top layer of plasma to a new tube and then frozen at -80°C in 1ml aliquots.

Isolation of plasma extracellular vesicles by size exclusion chromatography (SEC)

Frozen platelet poor plasma was removed from the freezer, thawed on ice and centrifuged at 2,000xg for 10 min to pellet debris. The plasma was then transferred to a new microcentrifuge tube and centrifuged at 10,000xg for 10min to pellet larger vesicles. Following centrifugation the plasma was transferred to a new tube and placed on ice until

analysis. Extracellular vesicle isolation was performed using a qEV 2.0 size exclusion chromatography column (Izon Science, Christchurch, New Zealand) following the manufactures protocol. Briefly, SEC columns were equilibrated to room temperature and flushed with 90ml of phosphate buffered saline (PBS) before use. Platelet poor plasma (time course analysis: 1.2ml, all other experiments: 2.0ml) was transferred into the sample loading reservoir of the SEC column. The column cap was then removed and the plasma sample was allowed to completely enter the column, at which point the sample loading reservoir was filled with PBS. The first 13ml of PBS fraction was discarded and the following 8ml's of EV containing fraction were collected for each sample. The SEC columns were then flushed with 90ml of PBS before the addition of the next sample. The 8ml of EV containing fraction for each sample was then pelleted by ultracentrifugation at 20,000 x g to pellet LEVs. The supernatant was then transferred to a new ultracentrifugation tube and SEVs were pelleted at 100,000xg for 1.5hr at 4°C. Following ultracentrifugation the supernatant was discarded and all residual PBS was removed before tryptic digestion.

Protein digestion and label free mass spectrometry analysis

EV pellets were precipitated with the addition of 50µl of methanol. The methanol was then evaporated in a SpeedVac (Thermo Scientific, Waltham MA) and protein was reconstituted with 50µl of 50mM Tris pH 8.2 containing 0.002% zwittergent Z3-16 (EMD Millipore, Burlington MA) and subsequently heated at 95°C for 10min. 5ul of 110mM DTT (5mM final) was then added to reduce disulfide bonds and the samples were heated

at 70°C for 10min. Samples were then equilibrated back to room temperature over 20 minutes before alkylation with 5µl 120mM IAA (10mM final) and incubated for 30min protected from light. Following alkylation 0.1µg of Trypsin LysC mix was added, the samples were vortexed and then incubated at 37°C for 16hr. Finally, the digestion was terminated by adding 5µl of 5.25% TFA.

LC-MS conditions

Digested samples (15µl) were loaded onto a 0.33µl OptiPak trap column (Optimize Technologies) packed with Halo C18 peptide ES stationary phase. The trap was then washed with an aqueous loading buffer composed of 0.2% FA and 0.05% TFA for 4 minutes at 10µl/min. After the wash, the 10-port valve was switched and peptides were flushed off of the trap onto a 25cm x 75µm PicoFrit (New Objective) analytical column packed with Waters BEH 1.7µm stationary phase using a Dionex UltiMate 3000 RSLC liquid chromatography (LC) system (Thermo Scientific). The analytical gradient for peptide separation began at 2% mobile phase B (MPB) and 98% mobile phase A (MPA) for 4min, MPB was then increased to 30% over 40min, raised to 40% MPB over 20min, increased to 95% over 10min, held for 2min, returned to 2% B in one minute and equilibrated for 15min. MPA was composed of 98:2 (water/acetonitrile) with 0.2% FA and MPB was composed of 80:10:10 (acetonitrile/ isopropyl alcohol/water) with 0.2% FA. Analysis of the eluting peptides was performed using an Orbitrap Fusion Lumos mass spectrometer (Thermo Scientific) operated in data dependent mode. Survey scans were acquired from 300-1400m/z with 120,000 resolving power and an AGC of 4e5 and max

fill time of 50ms. MS/MS scans of selected precursor ions were performed for a maximum of 3s or until the list was exhausted and dynamic exclusion was set to 45s. Quadrupole isolation for MS/MS scans was set at 0.7 m/z followed by fragmentation in the ion trap with "Rapid" scan speed and an ion target value of 5e4 and maximum injection time of 22ms using normalized collision energy of 28% from 200-1200 m/z. The monoisotopic precursor selection was set to peptide and charge states of 1, greater than 5, or unknown were excluded.

Data Analysis

MS raw files were processed in MaxQuant software version 1.6.12 Peptides were searched using the Andromeda search engine against the human Uniprot FASTA database downloaded July 24th, 2019. Cysteine carbamidomethylation was set as a fixed modification and N-terminal acetylation and methionine oxidation were set as variable modifications. Searches were performed with a false discovery rate of 1% for both peptides and proteins using a target-decoy approach. Peptide length was to at least 7 amino acids long and MS2 match tolerance was set to 0.5Da. Enzyme specificity was set to trypsin and a maximum of 2 missed cleavages were allowed. Protein data was extracted from the "proteinGroups.txt" file and differential quantitation was carried out using a generalized linear model as previously described (56).

Gene Ontology Over Representation Analysis

Gene ontology over representation analysis was preformed using WebGestalt software. Redundancy of enriched gene sets was then reduced with the affinity propagation

method using the R package apcluster and gene sets passing FDR (Benjamimi-Hochberg procedure ≤ 0.05) were reported.

Chapter 5: Conclusion

In summary, this dissertation describes the application of several analytical and bioinformatics based tools to study EV mediated intercellular communication in exercise, exercise resistance in obesity, and EVs as biomarkers of disease biology in multiple myeloma. Fist, we developed and characterized a platform to profile and quantify the proteome of plasma derived EVs, termed SEC-MS. We demonstrate that this method is superior to the current gold standard UTC and can reproducibly measure the abundance of EV proteins over a large dynamic range. We then applied this method to study the release of EVs after endurance and resistance exercise and use cell line studies to identify tissue specific EV proteins.

EVs are thought to mediate intercellular communication in several physiological and pathological states. Prior to determining the role of EVs obesity associated exercise resistance, the molecular alterations within muscle tissue at baseline and after exercise need to be extensively characterized. Therefore, we performed a multi-omics analysis of muscle biopsy samples to compare lean and obese individuals at baseline and in response to exercise. This study identified several important alterations in obese individuals. At baseline, we identified derangements in oxidative phosphorylation as well as deficits in protein translation, both of which have been previously characterized. We also identified novel alterations in phosphorylation and kinase activity, in which obese individuals had reduced activity of several important kinases. We also identified unique response to exercise at the transcript, protein, and phosphorylation level in lean and obese individuals.

Finally, multi-omics integration identified deficits in GSK3β signaling within obese individuals which will likely be the impetus for future studies of glycogen synthesis in obesity.

Finally, we leveraged SEC-MS to investigate EVs as biomarkers of disease biology in MM. This study found upregulation of two interesting proteins in MM relative to MGUS. In MM, TFRC and CD40 are upregulated in SEVs and LEVs respectively. The upregulation of these proteins may be associated with conditions within the tumor micro-environment, however, additional studies will be required to confirm these findings. Furthermore, many proteins are upregulated SEVs and LEVS in patients with standard cytogenetic risk relative. Functional enrichment analysis of these proteins suggests they are involved in immune function, which may indicate that high cytogenetic risk is associated with reduced adaptive immune function. Moreover, within LEVs we found CD40 to be upregulated in MM patients relative to MGUS, but only in patients with standard risk. In high risk MM patients, CD40 was undetectable, further indicating that high cytogenetic risk may be associated with impaired immune function.

In concussion, these studies have made significant contributions to research in several fields and will be the basis for exciting future studies.

References

1. Cocucci, E., and Meldolesi, J. (2015) Ectosomes and exosomes: shedding the confusion between extracellular vesicles. *Trends in Cell Biology* **25**, 364-372
2. Frühbeis, C., Helmig, S., Tug, S., Simon, P., and Krämer-Albers, E.-M. (2015) Physical exercise induces rapid release of small extracellular vesicles into the circulation. *Journal of Extracellular Vesicles* **4**, 10.3402/jev.v3404.28239
3. Vechetti Jr, I. J., Valentino, T., Mobley, C. B., and McCarthy, J. J. The role of extracellular vesicles in skeletal muscle and systematic adaptation to exercise. *The Journal of Physiology* **n/a**
4. Garber, C. E., Blissmer, B., Deschenes, M. R., Franklin, B. A., Lamonte, M. J., Lee, I.-M., Nieman, D. C., and Swain, D. P. (2011) Quantity and Quality of Exercise for Developing and Maintaining Cardiorespiratory, Musculoskeletal, and Neuromotor Fitness in Apparently Healthy Adults: Guidance for Prescribing Exercise. *Medicine & Science in Sports & Exercise* **43**, 1334-1359
5. Febbraio, M. A. (2017) Health benefits of exercise — more than meets the eye! *Nature Reviews Endocrinology* **13**, 72-74
6. Safdar, A., Saleem, A., and Tarnopolsky, M. A. (2016) The potential of endurance exercise-derived exosomes to treat metabolic diseases. *Nature Reviews Endocrinology* **12**, 504
7. Whitham, M., Parker, B. L., Friedrichsen, M., Hingst, J. R., Hjorth, M., Hughes, W. E., Egan, C. L., Cron, L., Watt, K. I., Kuchel, R. P., Jayasooriah, N., Estevez, E., Petzold, T., Suter, C. M., Gregorevic, P., Kiens, B., Richter, E. A., James, D. E., Wojtaszewski, J. F. P., and Febbraio, M. A. (2018) Extracellular Vesicles Provide a Means for Tissue Crosstalk during Exercise. *Cell Metabolism* **27**, 237-251.e234
8. Bhaskaran, K., Douglas, I., Forbes, H., dos-Santos-Silva, I., Leon, D. A., and Smeeth, L. (2014) Body-mass index and risk of 22 specific cancers: a population-based cohort study of 5·24 million UK adults. *The Lancet* **384**, 755-765
9. Choquet, H., and Meyre, D. (2011) Genetics of Obesity: What have we Learned? *Curr Genomics* **12**, 169-179
10. Castaño, C., Kalko, S., Novials, A., and Párrizas, M. (2018) Obesity-associated exosomal miRNAs modulate glucose and lipid metabolism in mice. *Proceedings of the National Academy of Sciences* **115**, 12158
11. Lei, L.-M., Lin, X., Xu, F., Shan, S.-K., Guo, B., Li, F.-X.-Z., Zheng, M.-H., Wang, Y., Xu, Q.-S., and Yuan, L.-Q. (2021) Exosomes and Obesity-Related Insulin Resistance. *Front Cell Dev Biol* **9**, 651996-651996
12. De Filippis, E., Alvarez, G., Berria, R., Cusi, K., Everman, S., Meyer, C., and Mandarino, L. J. (2008) Insulin-resistant muscle is exercise resistant: evidence for reduced response of nuclear-encoded mitochondrial genes to exercise. *Am J Physiol Endocrinol Metab* **294**, E607-614
13. Nilsson, M. I., Greene, N. P., Dobson, J. P., Wiggs, M. P., Gasier, H. G., Macias, B. R., Shimkus, K. L., and Fluckey, J. D. (2010) Insulin resistance syndrome blunts the mitochondrial anabolic response following resistance exercise. *Am J Physiol Endocrinol Metab* **299**, E466-474
14. Timmons, J. A., Knudsen, S., Rankinen, T., Koch, L. G., Sarzynski, M., Jensen, T., Keller, P., Scheele, C., Vollaard, N. B., Nielsen, S., Akerström, T., MacDougald, O. A., Jansson, E.,

Greenhaff, P. L., Tarnopolsky, M. A., van Loon, L. J., Pedersen, B. K., Sundberg, C. J., Wahlestedt, C., Britton, S. L., and Bouchard, C. (2010) Using molecular classification to predict gains in maximal aerobic capacity following endurance exercise training in humans. *J Appl Physiol (1985)* **108**, 1487-1496

15. Bouchard, C., An, P., Rice, T., Skinner, J. S., Wilmore, J. H., Gagnon, J., Pérusse, L., Leon, A. S., and Rao, D. C. (1999) Familial aggregation of VO(2max) response to exercise training: results from the HERITAGE Family Study. *J Appl Physiol (1985)* **87**, 1003-1008
16. Rennie, M. J. (2009) Anabolic resistance: the effects of aging, sexual dimorphism, and immobilization on human muscle protein turnover. *Appl Physiol Nutr Metab* **34**, 377-381
17. Kumar, V., Selby, A., Rankin, D., Patel, R., Atherton, P., Hildebrandt, W., Williams, J., Smith, K., Seynnes, O., Hiscock, N., and Rennie, M. J. (2009) Age-related differences in the dose-response relationship of muscle protein synthesis to resistance exercise in young and old men. *J Physiol* **587**, 211-217
18. Cuthbertson, D., Smith, K., Babraj, J., Leese, G., Waddell, T., Atherton, P., Wackerhage, H., Taylor, P. M., and Rennie, M. J. (2005) Anabolic signaling deficits underlie amino acid resistance of wasting, aging muscle. *Faseb j* **19**, 422-424
19. Dai, J., Su, Y., Zhong, S., Cong, L., Liu, B., Yang, J., Tao, Y., He, Z., Chen, C., and Jiang, Y. (2020) Exosomes: key players in cancer and potential therapeutic strategy. *Signal Transduction and Targeted Therapy* **5**, 145
20. Lemaire, M., Deleu, S., De Bruyne, E., Van Valckenborgh, E., Menu, E., and Vanderkerken, K. (2011) The microenvironment and molecular biology of the multiple myeloma tumor. *Adv Cancer Res* **110**, 19-42
21. Bianchi, G., and Munshi, N. C. (2015) Pathogenesis beyond the cancer clone(s) in multiple myeloma. *Blood* **125**, 3049-3058
22. Moloudizargari, M., Abdollahi, M., Asghari, M. H., Zimta, A. A., Neagoe, I. B., and Nabavi, S. M. (2019) The emerging role of exosomes in multiple myeloma. *Blood Reviews* **38**, 100595
23. Rajkumar, S. V., Dimopoulos, M. A., Palumbo, A., Blade, J., Merlini, G., Mateos, M.-V., Kumar, S., Hillengass, J., Kastritis, E., Richardson, P., Landgren, O., Paiva, B., Dispenzieri, A., Weiss, B., LeLeu, X., Zweegman, S., Lonial, S., Rosinol, L., Zamagni, E., Jagannath, S., Sezer, O., Kristinsson, S. Y., Caers, J., Usmani, S. Z., Lahuerta, J. J., Johnsen, H. E., Beksac, M., Cavo, M., Goldschmidt, H., Terpos, E., Kyle, R. A., Anderson, K. C., Durie, B. G. M., and Miguel, J. F. S. (2014) International Myeloma Working Group updated criteria for the diagnosis of multiple myeloma. *The Lancet Oncology* **15**, e538-e548
24. Korutla, L., Rickels, M. R., Hu, R. W., Freas, A., Reddy, S., Habertheuer, A., Harmon, J., Korutla, V., Ram, C., Naji, A., and Vallabhajosyula, P. Noninvasive diagnosis of recurrent autoimmune type 1 diabetes after islet cell transplantation. *American Journal of Transplantation* **0**
25. van Niel, G., D'Angelo, G., and Raposo, G. (2018) Shedding light on the cell biology of extracellular vesicles. *Nature Reviews Molecular Cell Biology* **19**, 213
26. Minciacchi, V. R., Freeman, M. R., and Di Vizio, D. (2015) Extracellular Vesicles in Cancer: Exosomes, Microvesicles and the Emerging Role of Large Oncosomes. *Seminars in Cell & Developmental Biology* **40**, 41-51
27. Wu, A. Y.-T., Ueda, K., and Lai, C. P.-K. (2019) Proteomic Analysis of Extracellular Vesicles for Cancer Diagnostics. *PROTEOMICS* **19**, 1800162

28. Kowal, J., Arras, G., Colombo, M., Jouve, M., Morath, J. P., Primdal-Bengtson, B., Dingli, F., Loew, D., Tkach, M., and Théry, C. (2016) Proteomic comparison defines novel markers to characterize heterogeneous populations of extracellular vesicle subtypes. *Proceedings of the National Academy of Sciences* **113**, E968-E977
29. György, B., Módos, K., Pállinger, É., Pálóczi, K., Pásztói, M., Misják, P., Deli, M. A., Sipos, Á., Szalai, A., Voszka, I., Polgár, A., Tóth, K., Csete, M., Nagy, G., Gay, S., Falus, A., Kittel, Á., and Buzás, E. I. (2011) Detection and isolation of cell-derived microparticles are compromised by protein complexes resulting from shared biophysical parameters. *Blood* **117**, e39-e48
30. Bard, M. P., Hegmans, J. P., Hemmes, A., Luider, T. M., Willemsen, R., Severijnen, L.-A. A., van Meerbeeck, J. P., Burgers, S. A., Hoogsteden, H. C., and Lambrecht, B. N. (2004) Proteomic Analysis of Exosomes Isolated from Human Malignant Pleural Effusions. *American Journal of Respiratory Cell and Molecular Biology* **31**, 114-121
31. Livshits, M. A., Khomyakova, E., Evtushenko, E. G., Lazarev, V. N., Kulemin, N. A., Semina, S. E., Generozov, E. V., and Govorun, V. M. (2015) Isolation of exosomes by differential centrifugation: Theoretical analysis of a commonly used protocol. *Scientific Reports* **5**, 17319
32. Kuang, M., Tao, X., Peng, Y., Zhang, W., Pan, Y., Cheng, L., Yuan, C., Zhao, Y., Mao, H., Zhuge, L., Zhou, Z., Chen, H., and Sun, Y. (2019) Proteomic analysis of plasma exosomes to differentiate malignant from benign pulmonary nodules. *Clinical proteomics* **16**, 5-5
33. Turay, D., Khan, S., Diaz Osterman, C. J., Curtis, M. P., Khaira, B., Neidigh, J. W., Mirshahidi, S., Casiano, C. A., and Wall, N. R. (2016) Proteomic Profiling of Serum-Derived Exosomes from Ethnically Diverse Prostate Cancer Patients. *Cancer investigation* **34**, 1-11
34. Ghosh, A., Davey, M., Chute, I. C., Griffiths, S. G., Lewis, S., Chacko, S., Barnett, D., Crapoulet, N., Fournier, S., Joy, A., Caissie, M. C., Ferguson, A. D., Daigle, M., Meli, M. V., Lewis, S. M., and Ouellette, R. J. (2014) Rapid isolation of extracellular vesicles from cell culture and biological fluids using a synthetic peptide with specific affinity for heat shock proteins. *PLoS One* **9**, e110443-e110443
35. Böing, A. N., van der Pol, E., Grootemaat, A. E., Coumans, F. A. W., Sturk, A., and Nieuwland, R. (2014) Single-step isolation of extracellular vesicles by size-exclusion chromatography. *Journal of extracellular vesicles* **3**, 10.3402/jev.v3403.23430
36. Kreimer, S., and Ivanov, A. R. (2017) Rapid Isolation of Extracellular Vesicles from Blood Plasma with Size-Exclusion Chromatography Followed by Mass Spectrometry-Based Proteomic Profiling. *Methods Mol Biol* **1660**, 295-302
37. Corso, G., Mäger, I., Lee, Y., Görgens, A., Bultema, J., Giebel, B., Wood, M. J. A., Nordin, J. Z., and Andaloussi, S. E. (2017) Reproducible and scalable purification of extracellular vesicles using combined bind-elute and size exclusion chromatography. *Scientific reports* **7**, 11561-11561
38. Karimi, N., Cvjetkovic, A., Jang, S. C., Crescitelli, R., Hosseinpour Feizi, M. A., Nieuwland, R., Lötvall, J., and Lässer, C. (2018) Detailed analysis of the plasma extracellular vesicle proteome after separation from lipoproteins. *Cell Mol Life Sci* **75**, 2873-2886
39. Jeannin, P., Chaze, T., Giai Gianetto, Q., Matondo, M., Gout, O., Gessain, A., and Afonso, P. V. (2018) Proteomic analysis of plasma extracellular vesicles reveals mitochondrial stress upon HTLV-1 infection. *Scientific Reports* **8**, 5170

40. Artoni, A., Merati, G., Padovan, L., Scalambrino, E., Chantarangkul, V., and Tripodi, A. (2012) Residual platelets are the main determinants of microparticles count in frozen-thawed plasma. *Thrombosis Research* **130**, 561-562
41. György, B., Szabó, T. G., Turiák, L., Wright, M., Herczeg, P., Lédeczi, Z., Kittel, Á., Polgár, A., Tóth, K., Dérfalvi, B., Zelenák, G., Böröcz, I., Carr, B., Nagy, G., Vékey, K., Gay, S., Falus, A., and Buzás, E. I. (2012) Improved Flow Cytometric Assessment Reveals Distinct Microvesicle (Cell-Derived Microparticle) Signatures in Joint Diseases. *PLoS One* **7**, e49726
42. LaCroix, R., JUDICONE, C., PONCELET, P., ROBERT, S., ARNAUD, L., SAMPOL, J., and DIGNAT-GEORGE, F. (2012) Impact of pre-analytical parameters on the measurement of circulating microparticles: towards standardization of protocol. *Journal of Thrombosis and Haemostasis* **10**, 437-446
43. Ayers, L., Kohler, M., Harrison, P., Sargent, I., Dragovic, R., Schaap, M., Nieuwland, R., Brooks, S. A., and Ferry, B. (2011) Measurement of circulating cell-derived microparticles by flow cytometry: Sources of variability within the assay. *Thrombosis Research* **127**, 370-377
44. Burnouf, T., Goubran, H. A., Chou, M.-L., Devos, D., and Radosevic, M. (2014) Platelet microparticles: Detection and assessment of their paradoxical functional roles in disease and regenerative medicine. *Blood Reviews* **28**, 155-166
45. Stranska, R., Gysbrechts, L., Wouters, J., Vermeersch, P., Bloch, K., Dierickx, D., Andrei, G., and Snoeck, R. (2018) Comparison of membrane affinity-based method with size-exclusion chromatography for isolation of exosome-like vesicles from human plasma. *J Transl Med* **16**, 1-1
46. Lacroix, R., Judicone, C., Mooberry, M., Boucekine, M., Key, N. S., Dignat-George, F., and The, I. S. S. C. W. (2013) Standardization of pre-analytical variables in plasma microparticle determination: results of the International Society on Thrombosis and Haemostasis SSC Collaborative workshop. *Journal of thrombosis and haemostasis : JTH*, 10.1111/jth.12207
47. Keerthikumar, S., Chisanga, D., Ariyaratne, D., Al Saffar, H., Anand, S., Zhao, K., Samuel, M., Pathan, M., Jois, M., Chilamkurti, N., Gangoda, L., and Mathivanan, S. (2016) ExoCarta: A Web-Based Compendium of Exosomal Cargo. *Journal of Molecular Biology* **428**, 688-692
48. Sasaki, T., Brakebusch, C., Engel, J., and Timpl, R. (1998) Mac-2 binding protein is a cell-adhesive protein of the extracellular matrix which self-assembles into ring-like structures and binds beta1 integrins, collagens and fibronectin. *The EMBO journal* **17**, 1606-1613
49. Tan, K., Duquette, M., Liu, J.-H., Zhang, R., Joachimiak, A., Wang, J.-h., and Lawler, J. (2006) The structures of the thrombospondin-1 N-terminal domain and its complex with a synthetic pentameric heparin. *Structure (London, England : 1993)* **14**, 33-42
50. Kakhniashvili, D. G., Bulla, L. A., and Goodman, S. R. (2004) The Human Erythrocyte Proteome. *Molecular & Cellular Proteomics* **3**, 501
51. Shen, X., Shen, S., Li, J., Hu, Q., Nie, L., Tu, C., Wang, X., Poulsen, D. J., Orsburn, B. C., Wang, J., and Qu, J. (2018) IonStar enables high-precision, low-missing-data proteomics quantification in large biological cohorts. *Proceedings of the National Academy of Sciences* **115**, E4767-E4776
52. Tabb, D. L., Vega-Montoto, L., Rudnick, P. A., Variyath, A. M., Ham, A.-J. L., Bunk, D. M., Kilpatrick, L. E., Billheimer, D. D., Blackman, R. K., Cardasis, H. L., Carr, S. A., Clauser, K. R., Jaffe, J. D., Kowalski, K. A., Neubert, T. A., Regnier, F. E., Schilling, B., Tegeler, T. J., Wang, M., Wang, P., Whiteaker, J. R., Zimmerman, L. J., Fisher, S. J., Gibson, B. W., Kinsinger, C.

R., Mesri, M., Rodriguez, H., Stein, S. E., Tempst, P., Paulovich, A. G., Liebler, D. C., and Spiegelman, C. (2010) Repeatability and Reproducibility in Proteomic Identifications by Liquid Chromatography−Tandem Mass Spectrometry. *Journal of Proteome Research* **9**, 761-776

53. Al Shweiki, M. H. D. R., Mönchgesang, S., Majovsky, P., Thieme, D., Trutschel, D., and Hoehenwarter, W. (2017) Assessment of Label-Free Quantification in Discovery Proteomics and Impact of Technological Factors and Natural Variability of Protein Abundance. *Journal of Proteome Research* **16**, 1410-1424
54. Uhlén, M., Fagerberg, L., Hallström, B. M., Lindskog, C., Oksvold, P., Mardinoglu, A., Sivertsson, Å., Kampf, C., Sjöstedt, E., Asplund, A., Olsson, I., Edlund, K., Lundberg, E., Navani, S., Szigyarto, C. A., Odeberg, J., Djureinovic, D., Takanen, J. O., Hober, S., Alm, T., Edqvist, P. H., Berling, H., Tegel, H., Mulder, J., Rockberg, J., Nilsson, P., Schwenk, J. M., Hamsten, M., von Feilitzen, K., Forsberg, M., Persson, L., Johansson, F., Zwahlen, M., von Heijne, G., Nielsen, J., and Pontén, F. (2015) Proteomics. Tissue-based map of the human proteome. *Science* **347**, 1260419
55. Frühbeis, C., Helmig, S., Tug, S., Simon, P., and Krämer-Albers, E.-M. (2015) Physical exercise induces rapid release of small extracellular vesicles into the circulation. *Journal of extracellular vesicles* **4**, 28239-28239
56. Robinson, M. M., Dasari, S., Konopka, A. R., Johnson, M. L., Manjunatha, S., Esponda, R. R., Carter, R. E., Lanza, I. R., and Nair, K. S. (2017) Enhanced Protein Translation Underlies Improved Metabolic and Physical Adaptations to Different Exercise Training Modes in Young and Old Humans. *Cell Metabolism* **25**, 581-592
57. Chen, I.-H., Xue, L., Hsu, C.-C., Paez, J. S. P., Pan, L., Andaluz, H., Wendt, M. K., Iliuk, A. B., Zhu, J.-K., and Tao, W. A. (2017) Phosphoproteins in extracellular vesicles as candidate markers for breast cancer. *Proceedings of the National Academy of Sciences* **114**, 3175-3180
58. Zhang, H., Liu, J., Qu, D., Wang, L., Wong, C. M., Lau, C.-W., Huang, Y., Wang, Y. F., Huang, H., Xia, Y., Xiang, L., Cai, Z., Liu, P., Wei, Y., Yao, X., Ma, R. C. W., and Huang, Y. (2018) Serum exosomes mediate delivery of arginase 1 as a novel mechanism for endothelial dysfunction in diabetes. *Proceedings of the National Academy of Sciences* **115**, E6927-E6936
59. Pedersen, B. K., and Hoffman-Goetz, L. (2000) Exercise and the Immune System: Regulation, Integration, and Adaptation. *Physiological Reviews* **80**, 1055-1081
60. Prokopi, M., Pula, G., Mayr, U., Devue, C., Gallagher, J., Xiao, Q., Boulanger, C. M., Westwood, N., Urbich, C., Willeit, J., Steiner, M., Breuss, J., Xu, Q., Kiechl, S., and Mayr, M. (2009) Proteomic analysis reveals presence of platelet microparticles in endothelial progenitor cell cultures. *Blood* **114**, 723-732
61. Lobb, R. J., Becker, M., Wen Wen, S., Wong, C. S. F., Wiegmans, A. P., Leimgruber, A., and Möller, A. (2015) Optimized exosome isolation protocol for cell culture supernatant and human plasma. *Journal of Extracellular Vesicles* **4**, 27031
62. Cox, J., and Mann, M. (2008) MaxQuant enables high peptide identification rates, individualized p.p.b.-range mass accuracies and proteome-wide protein quantification. *Nature Biotechnology* **26**, 1367-1372

63. Tyanova, S., Temu, T., Sinitcyn, P., Carlson, A., Hein, M. Y., Geiger, T., Mann, M., and Cox, J. (2016) The Perseus computational platform for comprehensive analysis of (prote)omics data. *Nature Methods* **13**, 731-740
64. Flegal, K. M., Kruszon-Moran, D., Carroll, M. D., Fryar, C. D., and Ogden, C. L. (2016) Trends in Obesity Among Adults in the United States, 2005 to 2014. *JAMA* **315**, 2284-2291
65. Pi-Sunyer, X. (2009) The medical risks of obesity. *Postgrad Med* **121**, 21-33
66. Gallagher, E. J., and LeRoith, D. (2015) Obesity and Diabetes: The Increased Risk of Cancer and Cancer-Related Mortality. *Physiol Rev* **95**, 727-748
67. Wang, Y. C., McPherson, K., Marsh, T., Gortmaker, S. L., and Brown, M. (2011) Health and economic burden of the projected obesity trends in the USA and the UK. *Lancet* **378**, 815-825
68. Cawley, J., and Meyerhoefer, C. (2012) The medical care costs of obesity: an instrumental variables approach. *J Health Econ* **31**, 219-230
69. Beals, J. W., Burd, N. A., Moore, D. R., and van Vliet, S. (2019) Obesity Alters the Muscle Protein Synthetic Response to Nutrition and Exercise. *Frontiers in Nutrition* **6**
70. Tsintzas, K., Jones, R., Pabla, P., Mallinson, J., Barrett, D. A., Kim, D.-H., Cooper, S., Davies, A., Taylor, T., Chee, C., Gaffney, C., Loon, L. J. C. v., and Stephens, F. B. (2020) Effect of acute and short-term dietary fat ingestion on postprandial skeletal muscle protein synthesis rates in middle-aged, overweight, and obese men. *American Journal of Physiology-Endocrinology and Metabolism* **318**, E417-E429
71. Breininger, S. P., Malcomson, F. C., Afshar, S., Turnbull, D. M., Greaves, L., and Mathers, J. C. (2019) Effects of obesity and weight loss on mitochondrial structure and function and implications for colorectal cancer risk. *Proc Nutr Soc* **78**, 426-437
72. Krug, K., Mertins, P., Zhang, B., Hornbeck, P., Raju, R., Ahmad, R., Szucs, M., Mundt, F., Forestier, D., Jane-Valbuena, J., Keshishian, H., Gillette, M. A., Tamayo, P., Mesirov, J. P., Jaffe, J. D., Carr, S. A., and Mani, D. R. (2019) A Curated Resource for Phosphosite-specific Signature Analysis. *Mol Cell Proteomics* **18**, 576-593
73. Wang, X., Hu, Z., Hu, J., Du, J., and Mitch, W. E. (2006) Insulin resistance accelerates muscle protein degradation: Activation of the ubiquitin-proteasome pathway by defects in muscle cell signaling. *Endocrinology* **147**, 4160-4168
74. Bollinger, L. M., Powell, J. J. S., Houmard, J. A., Witczak, C. A., and Brault, J. J. (2015) Skeletal muscle myotubes in severe obesity exhibit altered ubiquitin-proteasome and autophagic/lysosomal proteolytic flux. *Obesity (Silver Spring)* **23**, 1185-1193
75. Shinoda, K., Ohyama, K., Hasegawa, Y., Chang, H. Y., Ogura, M., Sato, A., Hong, H., Hosono, T., Sharp, L. Z., Scheel, D. W., Graham, M., Ishihama, Y., and Kajimura, S. (2015) Phosphoproteomics Identifies CK2 as a Negative Regulator of Beige Adipocyte Thermogenesis and Energy Expenditure. *Cell Metab* **22**, 997-1008
76. Zhang, B., and Horvath, S. (2005) A general framework for weighted gene co-expression network analysis. *Stat Appl Genet Mol Biol* **4**, Article17
77. Langfelder, P., and Horvath, S. (2008) WGCNA: an R package for weighted correlation network analysis. *BMC Bioinformatics* **9**, 559
78. Mackenzie, R. W., and Elliott, B. T. (2014) Akt/PKB activation and insulin signaling: a novel insulin signaling pathway in the treatment of type 2 diabetes. *Diabetes Metab Syndr Obes* **7**, 55-64

79. Beurel, E., Michalek, S. M., and Jope, R. S. (2010) Innate and adaptive immune responses regulated by glycogen synthase kinase-3 (GSK3). *Trends Immunol* **31**, 24-31
80. Sun, T., Rodriguez, M., and Kim, L. (2009) Glycogen synthase kinase 3 in the world of cell migration. *Dev Growth Differ* **51**, 735-742
81. Wu, D., and Pan, W. (2010) GSK3: a multifaceted kinase in Wnt signaling. *Trends Biochem Sci* **35**, 161-168
82. Embi, N., Rylatt, D. B., and Cohen, P. (1980) Glycogen synthase kinase-3 from rabbit skeletal muscle. Separation from cyclic-AMP-dependent protein kinase and phosphorylase kinase. *Eur J Biochem* **107**, 519-527
83. Platholi, J., Federman, A., Detert, J. A., Heerdt, P., and Hemmings, H. C., Jr. (2014) Regulation of protein phosphatase 1I by Cdc25C-associated kinase 1 (C-TAK1) and PFTAIRE protein kinase. *J Biol Chem* **289**, 23893-23900
84. Chen, H., Fajol, A., Hoene, M., Zhang, B., Schleicher, E. D., Lin, Y., Calaminus, C., Pichler, B. J., Weigert, C., Häring, H. U., Lang, F., and Föller, M. (2016) PI3K-resistant GSK3 controls adiponectin formation and protects from metabolic syndrome. *Proceedings of the National Academy of Sciences* **113**, 5754-5759
85. McCubrey, J. A., Steelman, L. S., Bertrand, F. E., Davis, N. M., Sokolosky, M., Abrams, S. L., Montalto, G., D'Assoro, A. B., Libra, M., Nicoletti, F., Maestro, R., Basecke, J., Rakus, D., Gizak, A., Demidenko, Z. N., Cocco, L., Martelli, A. M., and Cervello, M. (2014) GSK-3 as potential target for therapeutic intervention in cancer. *Oncotarget* **5**, 2881-2911
86. Jensen, J., Tantiwong, P., Stuenæs, J. T., Molina-Carrion, M., DeFronzo, R. A., Sakamoto, K., and Musi, N. (2012) Effect of acute exercise on glycogen synthase in muscle from obese and diabetic subjects. *Am J Physiol Endocrinol Metab* **303**, E82-89
87. Krishnamurthy, M., Ayazi, F., Li, J., Lyttle, A. W., Woods, M., Wu, Y., Yee, S. P., and Wang, R. (2007) c-Kit in early onset of diabetes: a morphological and functional analysis of pancreatic beta-cells in c-KitW-v mutant mice. *Endocrinology* **148**, 5520-5530
88. Zhao, M., Jung, Y., Jiang, Z., and Svensson, K. J. (2020) Regulation of Energy Metabolism by Receptor Tyrosine Kinase Ligands. *Front Physiol* **11**, 354-354
89. Krug, K., Mertins, P., Zhang, B., Hornbeck, P., Raju, R., Ahmad, R., Szucs, M., Mundt, F., Forestier, D., Jane-Valbuena, J., Keshishian, H., Gillette, M. A., Tamayo, P., Mesirov, J. P., Jaffe, J. D., Carr, S., and Mani, D. R. (2019) A Curated Resource for Phosphosite-specific Signature Analysis*[S]. *Molecular & Cellular Proteomics* **18**, 576-593
90. Bindea, G., Mlecnik, B., Hackl, H., Charoentong, P., Tosolini, M., Kirilovsky, A., Fridman, W. H., Pagès, F., Trajanoski, Z., and Galon, J. (2009) ClueGO: a Cytoscape plug-in to decipher functionally grouped gene ontology and pathway annotation networks. *Bioinformatics* **25**, 1091-1093
91. Zingone, A., and Kuehl, W. M. (2011) Pathogenesis of monoclonal gammopathy of undetermined significance and progression to multiple myeloma. *Semin Hematol* **48**, 4-12
92. Quail, D. F., and Joyce, J. A. (2013) Microenvironmental regulation of tumor progression and metastasis. *Nature Medicine* **19**, 1423-1437
93. Daniels, T. R., Delgado, T., Rodriguez, J. A., Helguera, G., and Penichet, M. L. (2006) The transferrin receptor part I: Biology and targeting with cytotoxic antibodies for the treatment of cancer. *Clin Immunol* **121**, 144-158

94. Daniels, T. R., Ortiz-Sánchez, E., Luria-Pérez, R., Quintero, R., Helguera, G., Bonavida, B., Martínez-Maza, O., and Penichet, M. L. (2011) An antibody-based multifaceted approach targeting the human transferrin receptor for the treatment of B-cell malignancies. *J Immunother* **34**, 500-508
95. Jessica, B., Maria Teresa Sabrina, B., Maurilio, P., Isabella, F., Marta, C., Bergsagel, P. L., Clara, C., and Alessandro, C. (2015) Erythroblast apoptosis and microenvironmental iron restriction trigger anemia in the VK*MYC model of multiple myeloma. *Haematologica* **100**, 534-841
96. Malle, E., Sodin-Semrl, S., and Kovacevic, A. (2009) Serum amyloid A: an acute-phase protein involved in tumour pathogenesis. *Cell Mol Life Sci* **66**, 9-26
97. Wakai, M., Hayashi, R., Tanaka, S., Naito, T., Kumada, J., Nomura, M., Takigawa, H., Oka, S., Ueno, Y., Ito, M., and Chayama, K. (2020) Serum amyloid A is a better predictive biomarker of mucosal healing than C-reactive protein in ulcerative colitis in clinical remission. *BMC Gastroenterology* **20**, 85
98. Lovisa, F., Garbin, A., Crotti, S., Di Battista, P., Gallingani, I., Damanti, C. C., Tosato, A., Carraro, E., Pillon, M., Mafakheri, E., Romanato, F., Gaffo, E., Biffi, A., Bortoluzzi, S., Agostini, M., and Mussolin, L. (2021) Increased Tenascin C, Osteopontin and HSP90 Levels in Plasmatic Small Extracellular Vesicles of Pediatric ALK-Positive Anaplastic Large Cell Lymphoma: New Prognostic Biomarkers? *Diagnostics (Basel)* **11**, 253
99. Paiva, B., Mateos, M. V., Sanchez-Abarca, L. I., Puig, N., Vidriales, M.-B., López-Corral, L., Corchete, L. A., Hernandez, M. T., Bargay, J., de Arriba, F., de la Rubia, J., Teruel, A.-I., Giraldo, P., Rosiñol, L., Prosper, F., Oriol, A., Hernández, J., Esteves, G., Lahuerta, J. J., Bladé, J., Perez-Simon, J. A., San Miguel, J. F., and groups, o. b. o. t. G. E. d. M. P. d. E. y. T. d. l. H. M. c. s. (2016) Immune status of high-risk smoldering multiple myeloma patients and its therapeutic modulation under LenDex: a longitudinal analysis. *Blood* **127**, 1151-1162
100. Elgueta, R., Benson, M. J., de Vries, V. C., Wasiuk, A., Guo, Y., and Noelle, R. J. (2009) Molecular mechanism and function of CD40/CD40L engagement in the immune system. *Immunol Rev* **229**, 152-172